Published in final edited form as:

Pain. 2016 September ; 157(9): 2124–2140. doi:10.1097/j.pain.0000000000000628.

Sustained relief of ongoing experimental neuropathic pain by a CRMP2 peptide aptamer with low abuse potential

Jennifer Y. Xie[#], **Lindsey A. Chew**[#], **Xiaofang Yang**[#], **Yuying Wang**[#], **Chaoling Qu**[#], **Yue Wang**[#], **Lauren M. Federici**[¶], **Stephanie D. Fitz**[¶], **Matthew S. Ripsch**[‡], **Michael R. Due**[‡], **Aubin Moutal**[#], **May Khanna**[#], **Fletcher A. White**[¶,‡], **Todd W. Vanderah**[#,¢,††], **Philip L. Johnson**[¶,¥], **Frank Porreca**[#,††,*], and **Rajesh Khanna**[#,*]

[#]Department of Pharmacology, P.O. Box 245050, Tucson, Arizona 85724 USA

[¢]Department of Neurology, P.O. Box 245050, Tucson, Arizona 85724 USA

[††]Department of Anesthesiology, P.O. Box 245050, Tucson, Arizona 85724 USA

[‡]Department of Anesthesia, Indiana University School of Medicine, Indianapolis, Indiana, 46202 USA

[¶]Department of Anatomy and Cell Biology, Indiana University School of Medicine, Indianapolis, Indiana, 46202 USA

[¥]Department of Psychiatry, Indiana University School of Medicine, Indianapolis, Indiana, 46202 USA

Keywords

CRMP2; CaV2.2; constellation pharmacology; neuropathic pain; allodynia; dopamine release; nucleus accumbens; conditioned place preference

1. Introduction

N-type voltage-gated calcium channel (Cav2.2) is a validated target for chronic pain treatment [10; 94; 96]. These channels underlie increased excitability and neurotransmission accompanying pathological conditions including neuropathic pain [15; 21; 66]. ω-conotoxin GVIA (Ziconotide/Prialt®) is a selective tonic blocker of the closed-state of CaV2.2 and is used clinically by the intrathecal route of administration to treat neuropathic pain [84]. The use of ziconotide, however, is encumbered by difficult dosing regimens, a very narrow therapeutic window, and numerous side effects including dizziness, nausea, nystagmus, memory impairment, and hallucinations [68; 75; 76; 82]. Nevertheless, the clinical efficacy

[*]To whom correspondence should be addressed: Dr. Rajesh Khanna, Department of Pharmacology, College of Medicine, University of Arizona, 1501 North Campbell Drive, P.O. Box 245050, Tucson, AZ 85724, USA, Office phone: (520) 626-4281; Fax: (520) 626-2204; rkhanna@email.arizona.edu or Dr. Frank Porreca, Department of Pharmacology, College of Medicine, University of Arizona, 1501 North Campbell Drive, P.O. Box 245050, Tucson, AZ 85724, USA, Office phone: (520) 626-7421; Fax: (520) 626-2204; frankp@email.arizona.edu.

Conflict of interest – There is no conflict of interest for any of the authors.

of ziconotide, supports the development of novel CaV2.2-targeted compounds with superior properties [49; 95].

We reported that collapsin response mediator protein 2 (CRMP2) interacts with CaV2.2 and enhances its functional activity [14; 19; 44; 86]. CBD3, a peptide from CRMP2, disengages CaV2.2 from CRMP2 to inhibit calcium influx, transmitter release and acute, inflammatory and neuropathic pain [13] [28]. In seeking to improve upon this novel allosteric antagonism, we tailored CBD3 peptides with antinociceptive efficacy in models of postoperative pain [29], and neuropathic pain induced by anti-retroviral drug treatment [13; 70], or focal nerve demyelination [89]. A mutant CBD3 peptide, where the 6^{th} amino acid was changed from alanine to lysine, demonstrated suppression of nociceptor excitability and inhibition of not only N-, but also, T- and R-type Ca^{2+} channels and was efficacious in reversing neuropathic pain induced by anti-retroviral drug treatment [67]. Here, merging the pan-calcium channel inhibitory nature of the mutant peptide with the R9 motif, we created R9-CBD3-A6K.

To test the *in vivo* efficacy of R9-CBD3-A6K in mitigating nerve injury-induced neuropathic pain, a translatable output measure advanced by Porreca and group was applied [61; 93]. Assessment of ongoing pain has been challenging in nonverbal animals. Pain is aversive, producing strong motivational drive to escape or seek relief. We previously demonstrated that pairing a context with a treatment that effectively relieves ongoing pain produces preference for that context (i.e., conditioned place preference) through negative reinforcement. Removal of aversive states induced by ongoing pain by intrinsically non-rewarding treatments (e.g., peripheral nerve block with lidocaine or intravenous ketorolac [62; 69; 93]) are accompanied by release of dopamine in the nucleus accumbens (NAc) shell representing the natural reward of pain relief. Thus, assessment of NAc dopamine release was proposed as an objective, neurochemical translational biomarker of pain relief [24; 62; 69; 93]; this concept has been validated in post-surgical [61], cephalic [24], osteoarthritic [64], neuropathic [93], and cancer-induced bone [69] pain. Here, we tested if acute R9-CBD3-A6K induces DA release from NAc in nerve-injured, but not naïve or sham-operated, animals. We also evaluated whether tolerance is observed to the pain relief following sustained administration of R9-CBD3-A6K, and assessed potential CNS side effects including impairment of memory retrieval, sensorimotor function, or depression. Our studies characterize R9-CBD3-A6K as a novel allosterically modulator of CaV channels, with therapeutic potential to treat severe neuropathic pain with an acceptable safety profile.

2. Methods

2.1. Animals

Pathogen-free, adult female Sprague-Dawley rats (initial weight 150–200 g; Harlan Laboratories, Houston, TX) were housed in temperature (23 ± 3°C) and light (12-h light: 12-h dark cycle; lights on at 07:00 h) controlled rooms with standard rodent chow and water available *ad libitum*. There are very few studies using female animals in preclinical settings, despite many chronic pain conditions involving more female patients than male counterparts. The Institutional Animal Care and Use Committees of Indiana University/Purdue University in Indianapolis or the University of Arizona approved these experiments. All procedures were conducted in accordance with the Guide for Care and Use of Laboratory Animals

published by the National Institutes of Health, the ethical guidelines of the International Association for the Study of Pain. Study design followed the ARRIVE guidelines initially published by Journal of Pharmacology and Pharmacotherapeutics [45]. Animals were randomly assigned to treatment or control groups and experimenters were blinded to the grouping information until the analysis was completed.

2.2. Peptide, chemicals, and antibodies

R9-CBD3-A6K (RRRRRRRRRARSRLKELRGVPRGL) peptide was synthesized and HPLC-purified by Genscript Inc. (Piscataway, NJ). All chemicals, unless noted were purchased from Sigma (St. Louis, MO). Antibodies were purchased as follows: CRMP2 (Cat# C2993, Sigma, St. Louis, MO) and CaV2.2 (TA308673, Origene Technologies, Inc, Rockville, MD).

2.3. CRMP2 protein purification

GST-CRMP2 protein was purified as previously described [14; 85]. Briefly, following an 19 h long induction at 16°C with 0.5 mM IPTG, bacterial cells expressing recombinant CRMP2-GST were resuspended in 50 mM NaH_2PO_4, pH 7.5, 500 mM NaCl, 10% glycerol, 0.5 mM TCEP, supplemented with Complete EDTA-free protease inhibitors (Roche, Basel, Switzerland). Disruption of the bacteria was performed by two rounds of high-pressure homogenization at 10,000 PSI with a LM10 microfluidizer (Microfluidics, Westwood), and the lysate was centrifuged 45 min at 4,500Xg at 4°C. The supernatant was loaded on a GST-Trap HP column (GE Healthcare, Uppsala, Sweden) equilibrated with 50 mM HEPES pH 7.5, 300 mM NaCl, 10% glycerol, and 0.5 mM TCEP. After a washing step with 50 mM HEPES pH 7.5, 300 mM NaCl, 10% glycerol, 0.5 mM TCEP, CRMP2-GST was eluted with a glutathione gradient. The fractions of interest for CRMP2-GST were loaded on a HiLoad Superdex size exclusion column (GE Healthcare, Uppsala, Sweden) and eluted with 50 mM NaH_2PO_4, pH 7.5 10% glycerol, 0.5 mM TCEP. The eluted proteins were concentrated with Amicon Ultra 15 centrifugal filters (Regenerated cellulose 10,000 NMWL; Merck Millipore, Darmstadt, Germany) and flash frozen on dry ice and stored at −80°C until use. Protein concentration was determined by a Pierce assay using bovine serum albumin (BSA) as a standard. The purity of the protein was verified with SDS-PAGE and structure/activity by checking its ability to bind tubulin (data not shown).

2.4. GST-pull-down and Western blotting

Lumbar segment of spinal cord lysates prepared from adult Sprague Dawley rats were generated by homogenization and sonication in RIPA buffer (50 mM Tris-HCl, pH 7.4, 50 mM NaCl, 2 mM $MgCl_2$, 1% (vol/vol) NP40, 0.5% (mass/vol) sodium deoxycholate, 0.1% (mass/vol) SDS). The RIPA buffer included freshly added protease inhibitors (Cat# B14002, Biotools, Houston, TX), phosphatase inhibitors (Cat# B15002, Biotools, Houston, TX), and Benzonase (Cat# 71206, Millipore, Billerica, MA). Protein concentrations were determined using the BCA protein assay (Cat# PI23225, Thermo scientific). Glutathione magnetic beads (Cat# B23702, Biotools, Houston, TX), pre-incubated with purified CRMP2-GST (~0.4 μM), were incubated overnight with 300 μg of total protein from spinal cord lysates at 4°C in the absence or presence of the indicated peptides with gentle rotation. Beads were washed 3 times with RIPA buffer before re-suspension in Laemmli buffer and denaturation (5 min at

95°C) and immunoblotting [12; 42; 90]. Immunoblots were revealed by enhanced luminescence (WBKLS0500, Millipore) before exposure to photographic film. Films were scanned, digitized, and quantified using Un-Scan-It gel version 6.1 scanning software (Silk Scientific Inc, Orem, UT).

2.5. Preparation of acutely dissociated dorsal root ganglion (DRG) neurons

DRGs from all levels were acutely dissociated using methods as described previously [29]. Briefly, DRGs were removed from naïve animals. The DRGs were treated with collagenase A and collagenase D in HBSS for 20 min (1 mg/ml; Roche Applied Science, Indianapolis, IN), followed by treatment with papain (30 U/ml, Worthington Biochemical, Lakewood, NJ) in HBSS containing 0.5 mM EDTA and cysteine at 35 C. The cells were then dissociated by mechanical trituration in culture media containing 1 mg/ml bovine serum albumin and trypsin inhibitor (Worthington Biochemical, Lakewood, NJ). The culture media was Ham's F-12 mixture, DMEM, supplemented with 10% fetal bovine serum, penicillin and streptomycin (100 μg/ml and 100 U/ml) and N2 (Life Technologies). The cells were then plated on coverslips coated with poly-L lysine and laminin (BD bioscience) and incubated for 2–3 h before more culture media was added to the wells. The cells were then allowed to sit undisturbed for 12–15 h to adhere at 37° C (with 5% CO_2).

2.6.1. Surface biotinylation on live DRGs in culture—Biotinylation was performed as described previously [12; 13; 41]. DRGs were processed for biotinylation experiments 48 h post isoaltion. Briefly, live cells were incubated with sulfosuccinimidyl 2-(Biotinamido) Ethyl-1,3′Dithiopropionate (EZ-link Sulfo NHS-SS-biotin; 1 mg/mg protein, Pierce Biotechnology Inc., Rockland, IL) for 30 min at 4°C in cold PBS, pH 8.0. Excess biotin was quenched with PBS containing 100 mM glycine, washed 3× with ice-cold PBS and the pellet was resuspended in RIPA lysis buffer. The resuspended pellet was triturated 10× (25-gauge needle) and centrifuged at 100,000 × **g** for 20 min. The biotinylated proteins were separated from clear solubilizate by adsorption onto Streptavidin agarose beads (Novagen) for 2–4 h at 4°C. Beads were washed 3–5× with RIPA buffer, and bound biotinylated proteins were gently eluted off the beads with RIPA buffer containing 2% Triton X-100 and 650 mM NaCl by end-over-end incubation for 1 h at 30°C. The biotinylated and total fractions were subjected to immunoblotting with β-tubulin and CaV2.2 antibodies.

2.6.2. Immunocytochemistry, confocal microscopy and colocalization analysis —Immunocytochemistry was performed on DRGs incubated with vehicle (control) or peptide (30 μM) for 24 hr [14; 19; 29]. Briefly, cells were fixed using 4% paraformaldehyde, 4% sucrose for 20 min at room temperature. Permeabilization was achieved by a 30 min incubation in phosphate buffered saline (PBS), 0.1% Triton X-100, following which non-specific binding sites were saturated by PBS containing 3% bovine serum albumin for 30 min at room temperature. Cell staining was performed with primary antibodies (CaV2.2 and CRMP2) in PBS with 3% BSA overnight at 4°C. The cells were then washed thrice in PBS, and incubated with PBS containing 3% BSA and secondary antibodies (Alexa 488 goat anti-mouse and Alexa 594 goat anti-rabbit secondary antibodies (Life Technologies)) for 1 hr at room temperature. Coverslips were mounted and stored at 4°C until analysis. Immunofluorescent micrographs were acquired on a Ziess LSM 710 inverted upright

microscope using a 40X, 1.3 numerical aperture oil immersion objective or on a Nikon C1si scanning confocal microscope using CFI Plan APO VC 60× Oil immersion objective with 1.4 numerical aperture. For all quantitative comparisons among cells under differing experimental conditions, camera gain and other relevant settings were kept constant. Nikon NIS-elements software was used for quantifying cellular membrane fluorescence. Membrane immunoreactivity was calculated by measuring the signal intensity in the area contiguous to the boundary of the cell. Annular regions of interest (ROI) were assigned to individual neurons. A perimeter of a neuron was manually traced, and then an inner curve was obtained at a constant distance from the perimeter. A region enclosed by the two curves represented the annular membrane ROI. All images were corrected for background by subtracting the average background fluorescence (areas within the field of view not containing cells) from the region of interest. Finally, co-localization analysis, including calculation of the Pearson's correlation coefficient, was performed using the NIS-elements software.

2.7. Calcium imaging in acutely dissociated dorsal root ganglion neurons

DRG neurons were loaded at 37°C with 3 μM Fura-2AM (K_d=25 μM, λ_{ex} 340, 380 nm/λ_{emi} 512 nm) to follow changes in intracellular calcium ($[Ca^{2+}]_c$) in a standard bath solution containing 139 mM NaCl, 3 mM KCl, 0.8 mM $MgCl_2$, 1.8 mM $CaCl_2$, 10 mM NaHEPES, pH 7.4, 5 mM glucose exactly as previously described [13]. Fluorescence imaging was performed with an inverted microscope, Nikon Eclipse TE2000-U, using objective Nikon Super Fluor 20× 0.75 NA and a Photometrics cooled CCD camera CoolSNAPHQ (Roper Scientific, Tucson, AZ) controlled by MetaFluor 6.3 software (Molecular Devices, Downingtown, PA). The excitation light was delivered by a Lambda-LS system (Sutter Instruments, Novato, CA). The excitation filters (340 ± 5 and 380 ± 7) were controlled by a Lambda 10-2 optical filter change (Sutter Instruments). Fluorescence was recorded through a 505 nm dichroic mirror at 535 ± 25 nm. To minimize photobleaching and phototoxicity, the images were taken every ~5 seconds during the time-course of the experiment using the minimal exposure time that provided acceptable image quality. The changes in $[Ca^{2+}]_c$ were monitored by following a ratio of F340/F380, calculated after subtracting the background from both channels.

2.8. Constellation pharmacology

These experiments were performed as described previously [57; 80], but with the following modifications. DRG neurons were loaded at 37°C with 3μM Fura-2AM for 30 minutes in Tyrode's solution. After a 1 minute baseline measurement Ca^{2+} influx was stimulated by the addition of the following receptor agonists: 400 nM menthol, 50 μM histamine, 10 μM adenosine triphosphate (ATP), 200 μM allyl isothiocyanate (AITC), 1 mM acetylcholine (Ach), 100 nM capsaicin diluted in Tyrode's solution (without TTX or Nifedipine). At the end of the constellation pharmacology protocol, cell viability was assessed by depolarization-induced Ca^{2+} influx using and an excitatory KCl solution comprised of 32mM NaCl, 90mM KCl, 2mM $MgCl_2$, 2mM $CaCl_2$, 25mM HEPES, pH 7.4, 30mM glucose. After the 1-minute baseline measurement, each trigger was applied for 15-seconds in the order indicated above in 6-minute intervals. Following each trigger, bath solution was continuously perfused over the cells to wash off excess of the trigger. This process was automated using the software WinTask x64 (Version 5.1, WinTask) that controlled the

perfusion of the standard bath solution and triggers through Valvelink 8.2 software (Automate Scientific). For the R9-CBD3-A6K condition, 10-μM peptide was added to the Tyrode's solution during the loading with Fura-2AM, as well as to each of the solutions containing a trigger. Fluorescence imaging was performed under the same conditions noted above for calcium imaging. A cell was defined as a 'responder' if its fluorescence ratio of 340nm/380nm was greater than 10% of the baseline value calculated using the average fluorescence in the 30 seconds preceding application of the trigger.

2.9. Electrophysiology

2.9.1. Current clamp electrophysiology—Electrophysiology experiments were performed as described previously [67]. Sharp-electrode intracellular recordings were obtained from primary DRG neurons 12–18 h after dissociation. Coverslips were transferred to a recording chamber that was mounted on the stage of an inverted microscope (Nikon Eclipse Ti, Nikon Instruments Inc., Melville, NY). The chamber was perfused with a bath solution containing (mM): NaCl 120, KCl 3, CaCl2 1, MgCl2 1, HEPES 10, Glucose 10, adjusted to pH 7.4 and osmolarity 300 mosM. The recordings were obtained at room temperature. Intracellular recording electrodes were fabricated from borosilicate glass (World Precision Instruments, Sarasota, FL) and pulled on a Flaming/Brown micropipette puller (P-98, Sutter Instruments, Novato, CA). Electrodes were filled with 1.0 M KCl (impedance: 40–80 MΩ) and positioned by a micromanipulator (Newport Corporation, Irvine, CA). A −0.1 nA current injection was used to bridge-balance the electrode resistance. Electrophysiological recordings were performed with continuous current-clamp in bridge mode using an AxoClamp-2B amplifier, stored digitally via Digidata 1322A interface, and analyzed offline with pClamp 9 software (Axon Instruments, Union City, CA). A neuron was accepted for study only when it exhibited a resting membrane potential (RMP) more negative than −45 mV. For each neuron isolated for study, a continuous recording was obtained for 1 minute without the delivery of any external stimulus. Neuronal excitability of small (≤30 μm) and medium (31–45 μm) diameter dissociated DRG (lumbar) sensory neurons was measured by injecting 1-s current pulses into the soma every 30 s. Cell size was estimated during patch clamp experiments using an eyepiece micrometer and a 20× objective (Nikon Eclipse TE2000-U, using objective Nikon Super Fluor 20× 0.75 NA). At this magnification, one tick mark within the eyepeice micrometer is equivalent to 5.0 μm. Current was adjusted in order to elicit 1–2 action potentials per current injection under baseline conditions. Following 3 control current injections, R9-CBD3-A6K was applied to the coverslip and current injections continued every 30 s. Neuronal excitability was measured as number of action potentials elicited per current pulse before and immediately after addition of R9-CBD3-A6K (15 and 45 s, respectively).

2.9.2. Whole-cell voltage-clamp electrophysiology—Recordings were obtained from acutely dissociated DRG neurons as described [29]. To isolate calcium currents, Na^+ and K^+ currents were blocked with 500 nM tetrodotoxin (TTX; Alomone Laboratories) and 30 mM tetraethylammonium chloride (TEA-Cl; Sigma). Extracellular recording solution (at ~310 mOsm) consisted of the following (in mM): 110 *N*-methyl-D-glucamine (NMDG), 10 $BaCl_2$, 30 TEA-Cl, 10 HEPES, 10 glucose, pH at 7.4, 0.001 TTX, 0.01 nifedipine. The intracellular recording solution (at ~310 mOsm) consisted of the following (in mM):

contained 150 CsCl2, 10 HEPES, 5 Mg-ATP, 5 BAPTA, pH at 7.4. Fire-polished recording pipettes, 2 to 5 MV resistances were used for all recordings. Whole-cell recordings were obtained with a HEKA EPC-10 USB (HEKA Instruments Inc.); data were acquired with a Patchmaster (HEKA) and analyzed with a Fitmaster (HEKA). Capacitive artifacts were fully compensated, and series resistance was compensated by ~70%. Recordings made from cells with greater than a 5 mV shift in series resistance compensation error were excluded from analysis. All experiments were performed at room temperature (~23°C). To isolate the contributions of particular channel subtypes, we used the following subunit-selective blockers (all purchased from Alomone Labs, Jerusalem): Nifedipine (10 μM, L-type); ω-agatoxin GIVA (200 nM, P/Q-type) [56]; ω-conotoxin-GVIA (500 nM, N-type) [26]; SNX-482 (200 nM, R-type) [63]; and 3,5-dichloro-N-[1-(2,2-dimethyl-tetrahydro-pyran-4-ylmethyl)-4-fluoro-piperidin-4-ylmethyl]-benzamide (TTA-P2, 1 μM, T-type) [20].

2.10. Tibial Nerve Injury (TNI)

Tibial nerve injury (TNI) was carried out to model nerve injury-induced neuropathic pain as described previously [42; 90]. Female Sprague-Dawley rats 150–200g were anesthetized using isoflurane (4% induction and 2% maintenance). The right sciatic nerve was isolated under aseptic surgical conditions by blunt dissection of the femoral biceps muscle, without damaging the epimycium. The sciatic nerve and its three branches were isolated: the sural, common peroneal and tibial nerves and only the tibial nerve was tightly-ligated with 5-0 silk and transected distal to the ligation. Additional 2–3 mm of distal nerve stump was removed to prevent re-innervation by the proximal nerve. The overlying muscle and skin was then sutured in two separate layers. Sham-injured animals were subjected to all preceding procedures with the exception of ligation and transection.

2.11. Assessment of tactile hypersensitivity

In experiments conducted in Tucson, the withdrawal threshold of the hindpaw was determined in response to probing with a series of eight calibrated von Frey filaments (Stoelting, Wood Dale, IL) in logarithmically spaced increments ranging from 0.41 to 15 gm (4–150 N). Each filament was applied perpendicularly to the plantar surface of the left hindpaw of rats kept in suspended wire-mesh cages (20 × 15 × 20 cm with ~5 mm openings). Behavioral baseline measurements were taken before injury, prior to and after intraperitoneal administration of drug or vehicle. The duration of each stimulus was approximately 3 s and the inter-stimulus interval was approximately 15 s. Withdrawal threshold was determined by sequentially increasing and decreasing the stimulus strength (“up and down” method), analyzed using a Dixon nonparametric test [17], and expressed as the mean withdrawal threshold.

In experiments conducted in Indianapolis, mechanical stimuli were applied with seven filaments, each differing in the bending force delivered (10, 20, 40, 60, 80, 100, and 120 mN), and fitted with a flat tip and fixed diameter of 0.2 mm. The filaments were tested in order of ascending force, with each filament delivered for 1 second in sequence from the 1st to the 6th spot. The interstimulus interval was 10–15 seconds. The incidence of foot withdrawal was expressed as a percentage of six applications of each filament as a function of force. A Hill equation was fitted to the function (Origin version 6.0, Microcal Software)

relating the percentage of indentations eliciting a withdrawal to the force of indentation. From this equation, the threshold force was obtained and defined as the force corresponding to a 50% withdrawal rate [52].

2.12. Osmotic minipump delivery

All drugs or saline being studied were delivered by means of an osmotic minipump (model AP 2001D; nominal pump rate: 8 μl/h for 1 day; model AP1003D: 1μl/h for 3 days; Alzet, Braintree Science, USA) that was primed according to manufacturers specifications and implanted subcutaneously on post-injury day 21. Briefly, after having shaved the skin, animals were anesthetized in an induction chamber with a volatile anesthetic in oxygen (isoflurane 4%). Anesthesia was maintained in a semi-open system using a nose-cone (isoflurane 2%). The minipump was inserted through a transversal incision in the skin of the lower middle part of the back, its aperture directed towards the head. Immediately after implantation, animals were allowed to recover from anesthesia. Behavioral testing for animals subjected to the 24 h minipumps began 1 hour after pump implantation and was repeated at 2, 4, 8, 24, 25, 26, 28, and 32 h. Behavioral testing for animals subjected to 72 h minipump began 8 hour after pump implantation and was repeated at 10, 12, 24, 36, 48, 60, 72, 80 h. R9-CBD3-A6K was delivered at a doses of 0.17 mg/h (24 h pump) or 0.22 mg/h (72 h pump). Control minipumps that were implanted in injured animals delivered 0.12 ml of 0.9% NaCl/rat per day.

2.13. *In vivo* microdialysis to measure dopamine release from nucleus accumbens shell (NAc)

2.13.1. Intracranial cannulation—Stereotaxic surgeries were performed in anesthetized rats (ketamine/xylazine 80/12 mg/kg, i.p.; Western Medical Supply, Arcadia, CA/Sigma, St. Louis, MO) according to the brain atlas. A single guide cannula (AG-8, EICOM, San Diego, CA) was implanted into the left NAc shell (AP: bregma +1.7 mm; ML: midline −1.0 mm; DV: skull−6.0 mm). Stainless steel dummy cannulas were inserted to keep the guide cannula free of debris. After surgery, rats were housed individually and allowed to recover for 7 days. The placement of the guide cannula was verified histologically *post hoc*. Data from the animals with misplaced cannula were discarded (<5%).

2.13.2. *In vivo* microdialysis procedures—Microdialysis was done in awake, freely moving rats with sham surgery or with TNI [62; 93]. The microdialysis probe (AI-8-2, EICOM, San Diego, CA) was inserted into the NAc with 2 mm semipermeable membrane (MW cutoff: 20 kDa) projecting beyond the guide cannula and perfused at 2.0 μl/min with artificial cerebrospinal fluid (aCSF: 147.0 mM NaCl, 2.8 mM KCl, 1.2 mM $MgCl_2$ and 1.2 mM $CaCl_2$). After a 90 min washout period, 2 baseline and 6 treatment fractions (30 min/fraction) were collected into pre-chilled (4°C) amber Eppendorf tubes containing 1.5 μl 40× antioxidant solution (6.0 mM L-cysteine, 2.0 mM oxalic acid and 1.3% w/v glacial acetic acid) [37]. All rats were then injected with cocaine (20 mg/kg, i.p.) and dialysates collected for additional 60 min as a positive control.

2.13.3. HPLC quantification of dopamine—Fractions were analyzed using Agilent 1100 HPLC system (Agilent, USA) with a 5020 guard cell, MD-150 column and Coulochem

III 5014B electrochemical detector (Thermofisher; USA) at ambient temperature [93]. The guard cell was set at 350 mV, Electrode1 at −150 mV and Electrode2 at 250 mV. A standard curve was produced from 6 serial dilutions of DA (1.25 – 40 pg) in 20 μl aCSF plus antioxidant cocktail. The limit of detection (LOD) and limit of quantification (LOQ) were calculated according to the formulas: LOD = 3.3 (SDr/S); LOQ = 10 (SDr/S); where the standard deviation of the response SDr (SD of y-intercepts of regression lines) and the slope of the standard curve S were determined from the measurements of 10 independent standard curves. The LOD and LOQ for DA were determined to be 0.3 and 0.9 pg on column, respectively. The linearity of DA peaks was also validated. The integration of the DA peaks from HPLC chromatograms was performed by an experimenter blinded to the treatment groups.

DA concentrations in microdialysates were expressed as pg/μl. The percent change of the corresponding baseline level was calculated to normalize the variations of individual rats and allow for multiple comparisons. The data of Percent Change from Baseline (PCB) were then converted to area under the time effect curve (AUC) to reflect the integrated change of the treatments. Rats that had basal DA levels below LOQ in the dialysates, incorrect cannula placement, uneven baselines (defined as >50% difference in DA concentrations between the two baseline fractions), or failed to demonstrate an increase of > 100% over baseline levels post cocaine administration were excluded from data analysis (approximately 10%).

2.14. Assessment of abuse liability

Potential abuse liability was assessed with place conditioning in naïve rats as previously described [29; 48]. Three-chambered rat-CPP apparatus (San Diego Instruments, San Diego, CA) with the following modifications were used: (1) end chamber of horizontal black and white striped walls, smooth floor; (2) end chamber of black walls, rough floor; and (3) middle chamber of neutral gray walls and metal rod flooring. Female Sprague-Dawley rats (200–225 g, Harlan) were implanted with intracerebroventricular cannula (i.c.v.). Although we have previously observed penetration of tat-CBD3 into the brain after an intraperitoneal injection [13], here we chose the i.c.v. route so as to allow for the assessment of direct actions of the peptides on CNS regions associated with reward pathways. After a recovery period (7 days), rats were put in CPP boxes for 20-minute sessions and allowed to freely explore 2 end chambers and a middle transition zone with unique environmental cues in each end chamber. Baseline measurements were obtained for each rat on days 1 through 4. The average baseline per rat was determined across days and used to calculate the mean time spent in each chamber. Animals spending more than 80% of the total time in any chamber at baseline were excluded from the study. On days 5, 7, 9, 11, and 13, R9-CBD3-A6K (10 mg in 5 μL, i.c.v.) was paired with one of the end chambers, whereas rats were confined to that chamber for 20 minutes. On days 6, 8, 10, and 12, animals received an injection of vehicle (saline 5 mL, i.c.v.) paired with the opposite chamber. On days 13 to 14, in a peptide-free state, the total time spent by the rat was recorded and compared with baseline values for each chamber (paired t test). Preference was demonstrated if there was a significant increase in the total time spent in the conditioning chamber when compared to baseline values.

2.15. Assessment of potential CNS side effects

2.15.1. Light-Dark Box test as a measure of anxiety-associated behavior—For the light-dark box test (LDBT), there were two adjoined light and dark compartments boxes with a 7 cm square opening to allow mice to move between them. The black box was covered (20cm×40cm×30cm height) and the white box (20cm×40cm×30cm height) was open and illuminated (40 W). Each mouse was placed into the white compartment and the white compartment was video recorded for later analyses using ANY-maze software (version 4.75, Stoelting, Wood Dale, IL) which is a video tracking system designed to automate testing in behavioral experiments. The main parameters were duration of time spent in the light box; the latency to enter the dark box; and the number of transitions between the light and dark box.

2.15.2. Open-field test as a measure of anxiety-associated behavior—The open-field arena covered an area of 90 cm × 90 cm, with 40 cm high walls. The open-field arena was divided into a 6 × 6 grid of equally-sized squares using black tape (36 total squares) with 4 squares forming the center; 12 squares forming the middle perimeter; and 20 squares forming the outer perimeter. The test started by placing a rat in the center. The behavior of each mouse in the open-field arena was recorded on video and scored afterwards by an observer blind to the experimental treatment of each rat. Time spent in each region of the open-field was recorded.

2.15.3. Elevated plus maze (EPM) anxiety test as a measure of anxiety-associated behavior—Immediately following the LDBT, rats were place in the center area of the EPM where the two arms intersect. The EPM measures many relevant anxiety related behaviors such as: number of pokes and full entries into and duration spent in closed versus open arm. The arena dimensions are the following: each arm is 5 cm wide and 35.5 cm long, closed walls are 15 cm high. The arms and central platform of the apparatus are elevated to a height of 62 cm. Behavior was video recorded for later analyses using ANY-maze software (version 4.75, Stoelting, Wood Dale, IL) which is a video tracking system designed to automate testing in behavioral experiments. The main parameters were duration of time spent in the open and closed arm and number of entries into the arms.

2.15.4. Tail suspension test as a measure of depression-associated behavior —Immediately following the EPM test, the TST was conducted according to standard procedure [23] between 8:00 AM and 2:00 PM. Briefly, each mouse was suspended by the tail at a height of 40 cm by taping the rail to a horizontal bar so that the tail is vertical to the bar. Behavior was video recorded for 5 min and later analyzed by an experimenter who was blinded to the treatments. An animal was considered to be immobile when it did not show any movement and hanged passively. If a mouse climbed its tail the mouse was gently pulled back down and continue trial. Mice that climbed their tails for more than 20% of the trial (i.e. >60 seconds) were eliminated from the final analysis. Duration and frequency of immobility were the main parameters measured.

2.15.5. Novel object recognition test—The experimental apparatus consists of an open-field box (36 × 30 × 26 cm). The apparatus was located in a quiet room. All mice were

subjected to three phases: acclimation, acquisition and test, and scores were recorded. For acclimation, the mouse was placed into the open field box and allowed to explore freely for 10 minutes daily for three days. No objects were placed in the box during the acclimation trial. Following acclimation, the acquisition trial was conducted by placing the mouse in the field; two novel objects are symmetrically fixed to the floor of the box 5 cm from the walls. The objects were constructed from a ping-pong ball, a cylindrical bottle cover and a piece of Lego brick, which were different in shape and color but similar in size. Mice were allowed to explore the two objects for 10 minutes (day 4), and exploratory activity (i.e., the time spent exploring each object) was recorded. After 24 hours (day 5), mice are re-exposed to one of the objects of the acquisition phase, together with a novel object (not used in acquisition phase). Once again, animals were allowed to explore freely for 5 minutes and the time spent exploring each object is recorded. A mouse was considered to be involved in exploratory behavior when its head was oriented directly towards the object and within approximately 1–2 cm from it. For test data, the percentage of exploration time spent at the novel object was determined.

2.16. Statistical analyses

Differences between means were compared by either paired or unpaired two-tailed Student's t–tests. Behavioral threshold values were statistically analyzed for each foot separately and the significance of differences between the average of at least two pre-injection tests and the mean obtained for each post-injection test. In all tests, baseline data were obtained for the TNI-injured groups before drug or vehicle administration. Within each treatment group, post-administration means were compared with the baseline values by repeated measures analyses of variance (RMANOVA) followed by *post hoc* Tukey's multiple comparison test. One-way ANOVA *post hoc* Tukey's multiple comparison test was used to analyze the integrated area under the time effect curve (AUC) of microdialysis data. A p value of <0.05 was used to indicate statistical significance between treatment and non-treatment groups.

3. Results

3.1. Rationale for choice of R9-CBD3-A6K for studies

We previously reported that CBD3, a 15 amino acid fragment of CRMP2, disrupts the CRMP2–CaV2.2 interaction [13] irrespective of the cell penetrating motif it is appended to: the HIV-1 transactivator of transcription domain (TAT) [13], a myristate (Myr) tag [29], or homopolyarginine (R9) [42]. A point mutation within the CBD3 sequence that replaced the alanine residue at position 6 with a lysine (i.e., A6K), increased binding to CaV2.2 and displayed increased structural stability compared to wild type CBD3 peptide as assessed from peptide array and molecular dynamics simulations, respectively [67]. Importantly, R9 conjugated CBD3 reversed TNI-induced mechanical hypersensitivity [42]. Additionally, compared to wildtype CBD3, the A6K mutant version of CBD3 conjugated to TAT exhibited a greater propensity to reduce mechanical hypersensitivity induced by antiretroviral therapy [67]. These results provide a rationale for the testing of a novel peptide, R9 grafted onto the A6K mutant version of CBD3, to generate R9-CBD3-A6K, with the expectation that this chemical modification would result in superior cell-penetrating prowess of R9 [87] combined with the enhanced inherent stability of the A6K mutation [67] and its superior

anti-nociceptive potential [42] would produce a better antinociceptive peptide therapeutic compared to wildtype CBD3. We selected R9-CBD3-A6K here because of the reported ability of the A6K mutation to additionally affect R- and T-type calcium channels [67]. Both R- and T-type channels are important pain targets with R-type knockout mice exhibiting reduced responses to inflammatory pain [73] and antagonism of R- and T-type channels with small molecules resulting in reversal of neuropathic pain [25; 54]. Scramble and random sequence based peptides conjugated to various cargoes as controls have been previously studied as controls in molecular, biochemical and behavioral assays and shown to have no effects [13; 29; 42; 67].

3.2. R9-CBD3-A6K disrupts the CRMP2–CaV2.2 interaction and inhibits surface trafficking of CaV2.2 in DRGs

We previously showed that all cell penetrant forms of CBD3 inhibited the CRMP2–CaV2.2 interaction [13; 29; 42; 67]. Therefore, we first confirmed that the R9-CBD3-A6K could interfere with the CRMP2–CaV2.2 interaction. Rat spinal cord lysates were incubated with glutathione beads pre-adsorbed with purified CRMP2-GST in the presence of DMSO (0.3%, control) or increasing concentrations (1–100 μM) of R9-CBD3-A6K and then the CRMP2-bound proteins were recovered by boiling in Laemmli buffer in reducing conditions, followed by immunoblotting. Probing of the CRMP2-enriched fraction with a CaV2.2 antibody demonstrated a robust interaction between CaV2.2 and CRMP2 (Fig. 1A; top blot, *lane 2*). R9-CBD3-A6K, in a concentration-dependent manner, attenuated this interaction with greater than ~75% inhibition at 10 μM (Fig. 1A; *top blot* and Fig. 1B). These results demonstrate that the R9-conjugated mutant peptide retains its ability to efficiently uncouple the CRMP2–CaV2.2 interaction.

We previously demonstrated that overexpression of a plasmid expressing the CBD3 fragment of CRMP2 almost completely prevented surface expression of co-expressed CaV2.2 in a surrogate neuronal cell line [13]. Confocal microscopy confirmed that both TAT- and Myr-conjugated CBD3 peptides inhibited surface trafficking of CaV2.2 in DRGs [29]. Here, we asked if R9-CBD3-A6K could affect trafficking of CaV2.2 in live DRGs in culture. Acutely dissociated DRGs grown for 12 h in culture were incubated in the absence (control) or presence of increasing concentrations of R9-CBD3-A6K (1 to 100 μM) for 24 h and surface biotinylated proteins were enriched using streptavidin beads. CaV2.2 was detected in the streptavidin-enriched biotinylated fractions (Fig. 1C; top blot, *lanes 1–7*) with little to no detection of the cytosolic protein βIII-tubulin in these fractions verifying the integrity of the extracellular biotinylation (Fig. 1C; third blot from top, *lanes 1–7*). CaV2.2 surface expression was calculated as the ratio of the biotinylated to total CaV2.2 and then normalized to the neurons treated with control. R9-CBD3-A6K, in a concentration-dependent manner, reduced the surface fraction of CaV2.2 with ~70% inhibition at 3 and 10 μM (Fig. 1C, D; top blot, *lanes 3 and 4 compared to lanes 1 or 7*). Increasing the concentration beyond 30 μM did not have any further inhibitory effects.

Next, we used immunofluorescent microscopy to determine if R9-CBD3-A6K affected the subcellular localization of both proteins. Sensory neurons were incubated with R9-CBD3-A6K peptide for 30 min and examined for their labeling of CaV2.2 and CRMP2 with

specific antibodies. Visual inspection of the micrographs (Fig. 1E) demonstrated that, in control cells treated with vehicle, the fluorescent signals for both proteins appeared to overlap at the plasma membrane of the DRGs. As illustrated in Fig. 1E (*top right panel*), prominent CaV2.2 staining was observed within the membrane in the absence of peptide and this staining co-localized with CRMP2 (Fig. 1E, *top left panel*). The Pearson correlation coefficient (PCC) was used to quantify the degree of colocalization between the fluorophores for the two proteins; PCC relies on the deviation from the mean. The high PCC values verified the membrane colocalization (Fig. 1F). After 30 min of R9-CBD3-A6K peptide treatment, CaV2.2 labeling was largely absent from the membrane (Figs. 1E, *lower right panel*; Fig. 1F) in contrast to DMSO-treated cells (Figs. 1E, *lower left panel*; Fig. 1F). Taken together, these results suggest that biochemically, R9-CBD3-A6K's mechanism of action is to uncouple the CRMP2-CaV2.2 complex and prevent CaV2.2 from being targeted to the DRG neuronal membrane.

3.3. R9-CBD3-A6K inhibits K^+-evoked Ca^{2+} influx in sensory neurons

We previously reported that uncoupling the CaV2.2–CRMP2 interaction with TAT- [13] or R9-CBD3 [42] resulted in a reduction of depolarization-induced Ca^{2+}-influx in sensory neurons. Here, we asked if R9-CBD3-A6K could work similarly. Calcium imaging experiments performed with Fura-2AM on rat DRG neurons demonstrated that stimulation with high 90 mM KCl (a concentration at which only CaV2 channels are recruited [88]) produced a transient rise in intracellular calcium ($[Ca^{2+}]_c$) (Figure 2A). Peak calcium influx was recorded within 20 sec of stimulation (Fig. 2A, B). Calcium responses of DRGs, of small to large diameter neurons, incubated for 20 min with R9-CBD3-A6K were reduced, by ~50% in their peak (Fig. 2B, C) or integrated area under the curve (AUC) compared to control (Fig. 2D). These results demonstrate that R9-CBD3-A6K inhibits calcium influx via CaV2 channels (see also *section 3.6.*).

3.4. Functional 'fingerprinting' of sensory neurons treated with R9-CBD3-A6K reveals lack of off-target effects

Since R9-CBD3-A6K is a novel peptide, we set out to address to its potential side effects using a recently described phenotypic screening method termed constellation pharmacology [79; 80], which uses subtype-selective pharmacological agents to elucidate cell-specific combinations (constellations) of key signaling proteins that describe specific cell types. The constellation pharmacology protocol [57] consists of sequential challenges, applied 6-min apart, to test activity of Ca^{2+} permeable ligand-gated ion channels, metabotropic receptors and voltage-gated Ca^{2+} channels. At the end of each experiment, a membrane-depolarizing agent (i.e., KCl) is used to ensure neuronal viability; neurons that did not respond to this trigger were not analyzed. In each case the readout is a change in Ca^{2+} fluorescence. Typical responses to the challenges (Table 1) used are illustrated in Figure 3. Examples of typical Ca^{2+} traces of DRGs incubated with vehicle (0.002% DMSO) (Fig. 3A) or R9-CBD3-A6K (10 μM) (Fig. 3B) demonstrate the heterogeneity in responses. Importantly, consistent with our earlier data (Fig. 2), R9-CBD3-A6K reproducibly decreased the K^+-evoked Ca^{2+} influx despite being applied after several challenges of the constellation pharmacology protocol.

We applied the constellation pharmacology protocol [57] to DRG neurons treated for 30 min with 10 μM R9-CBD3-A6K (n=1301) or 0.002% DMSO (vehicle, n=1184) (Table 1). Data from 4 independent experiments were collected and the responses of each neuron to each constellation pharmacology trigger were analyzed. Only DRGs with responses >10% over the baseline fluorescence were considered in our analyses. We first asked if R9-CBD3-A6K treatment altered the overall competence of the neurons by assessing if the DRGs respond to the same number of agonist challenges, independently of which compound they responded to (Fig. 3C). In vehicle-treated DRGs, ~35% of cells responded to KCl only (labeled as 0 in radar plot in Fig. 3C), ~49% responded to KCl plus 1 other trigger (labeled 1 in Fig. 3C), and ~13% responded to KCl plus 2 other triggers (2 in Fig. 3C). The percent of neurons responding to more than 2 triggers was ≤ 3% (Supplementary Table 1). These percent responses were not altered by incubation with R9-CBD3-A6K (Fig. 3C, *red lines*), demonstrating that the peptide does not affect the overall capacity of sensory neurons to respond to agonist challenges.

We next asked if R9-CBD3-A6K could change the *sensitivity* of sensory neurons to the different agonist challenges. We determined the percent of cells responding to a defined trigger alone or to the defined trigger in combination with any other trigger(s). In vehicle-treated DRGs, the percent responders to the various triggers were: ~26% (Acetylcholine (Ach)), 2% (allyl isothiocyanate (AITC)), 17% ATP, 3% histamine, 5% menthol, and 33% capsaicin (Fig. 3D and Supplementary Table 1). The percent responders to these agonists were unchanged in cells treated with R9-CBD3-A6K ($p>0.05$, z-test) (Fig. 3D). In addition to the above classes, other major neuronal populations were also unchanged by R9-CBD3-A6K treatment (Fig. 3E and Supplementary Table 1). These results demonstrate that R9-CBD3-A6K does not target distinct neuronal populations.

3.5. Functional ‘fingerprinting’ and radioligand binding assays demonstrate selectivity of R9-CBD3-A6K

The above analyses do not take into account the extent of inhibition of Ca^{2+} influx following each challenge. Therefore, here we analyzed peak Ca^{2+} responses of responders to the various triggers. Agreeing with the inhibition in K^+-evoked Ca^{2+} influx observed in single trigger experiments earlier (Fig. 2), R9-CBD3-A6K again decreased K^+-evoked Ca^{2+} influx (~44% reduction compared to control, $p<0.001$) (Fig. 3F). Notably, compared to vehicle-treated neurons, the peak Ca^{2+} amplitude of R9-CBD3-A6K-treated DRGs was unchanged for all other triggers ($p>0.05$) except Ach (Fig. 3F). Area under the curve analyses of calcium influx (Fig. 3G) was similar to peak influx for all conditions except capsaicin: control 6.21 ± 0.35 (n=393) versus R9-CBD3-A6K 5.22 ± 0.27 (n=432). While this inhibition (~16%) is statistically significant and suggests a possible direct effect on vanilloid receptor 1 (VR1 or TRPV1), it may not be biologically relevant because of the differential access of capsaicin, a relatively hydrophobic molecule, across the lipid membrane. Additionally, because a previous study had reported that an arginine-rich hexapeptide blocks calcium influx via TRPV1 [36], we tested if the R9-CBD3-A6K peptide blocked these channels. Stimulation with 20 nM resiniferatoxin (RTX), a selective agonist of vanilloid receptors in nociceptive DRGs [16; 32; 91], induced a robust increase in $[Ca^{2+}]_c$ in ~15% (19 of 126) DRGs. RTX-induced $[Ca^{2+}]_c$ was unchanged in the presence of 10 μM of R9-

CBD3A6K ($p > 0.05$; one-way ANOVA with Tukey's post hoc test). Compared to vehicle-treated neurons, the peak and AUC Ca^{2+} amplitude of R9-CBD3-A6K-treated DRGs was also changed for Ach (Fig. 3F, G), suggesting an action via G-protein couple receptors on nicotinic acetylcholine receptors.

Primary radioligand binding profiles were also determined for R9-CBD3-A6K against a panel of 56 receptors, ion channels, and transporters, including adenosine, angiotensin, cannabinoid, serotonin, adrenergic, dopamine, GABA, histamine, muscarinic, melanocortin, neurokinin, neuropeptide Y, opioid, sigma, and transporters, and we saw no significant binding at 10 μM of R9-CBD3-A6K (Supplementary Table 2). R9-CBD3-A6K exhibited modest binding (~50–64% displacement at 10 μM) for muscarinic, neurokinin, and neuropeptide Y receptors, the small conductance Ca^{2+}-activated K^+ (SK_{Ca}) channel, and norepinephrine and dopamine receptors (Supplementary Table 2).

Collectively, these results triangulate to identify R9-CBD3-A6K as a selective inhibitor of calcium influx via CaV2 channels.

3.6. R9-CBD3-A6K inhibits Ca^{2+} currents in sensory neurons

We previously reported that TAT-CBD3 inhibits N- [13] and T-type [67] Ca^{2+} currents in sensory neurons, while the mutant TAT-CBD3-A6K peptide additionally inhibits R-type Ca^{2+} currents as well [67]. Here, we examined the effects of R9-CBD3-A6K on Ca^{2+} currents in sensory neurons. Acute application (30 min) of the R9-CBD3-A6K peptide inhibited total Ca^{2+} currents by ~63% (Fig. 4A, B); no changes were observed in activation or inactivation of these currents (data not shown). A further isolation of the currents using pharmacological blockers and appropriate voltage protocols, as described previously [67] (see also Methods), revealed a significant reduction of both T- (by ~40% compared to control) and R-type (by ~39% compared to control) Ca^{2+} currents (Fig. 4B). A similar level of inhibition (~33%) was observed using calcium imaging experiments in DRG neurons where we isolated Cav3 (T-type) channels using toxins selective for the other channels (control: 1.29 ± 0.05 (n=189) versus R9-CBD3-A6K: 0.87 ± 0.06 (n=121). The decrement in currents caused by acute application of R9-CBD3-A6K sets it apart from the myristoylated version of the peptide [29] and gabapentin, both of which were reported to unsuccessful in blocking currents following acute treatments [34].

3.7. Acute R9-CBD3-A6K suppresses excitability of nociceptive DRG neurons

We previously demonstrated inhibition of both T- and R-type Ca^{2+} macroscopic currents in sensory neurons by TAT-CDB3-A6K Similarly, R9-CBD3A6K was able to inhibit non-L-type, T- and R-type Ca^{2+} currents in DRG neurons (Fig. 4B). As both of these currents are important for controlling neuronal excitability [39; 55], we tested if R9-CBD3-A6K could affect neuronal excitability of dissociated DRG neurons. The excitability was measured by injecting current pulses (nA) into the soma of small diameter (≤30 μm) DRG neurons every 30 seconds in order to elicit 4–6 action potentials (average current injection of 0.6 ± 0.1 nA (n=16)) under control conditions prior to the addition of peptides into the recording bath. Representative recordings (Fig. 5A) and grouped data (Fig. 5B) show that the excitability of small diameter DRG neurons was decreased by R9-CBD3-A6K in a concentration-

dependent fashion. Five minutes following perfusion of R9-CBD3A6K, there was on average a ~85% reduction in the number of action potentials elicited by a current pulse compared to control (1.0 ± 0.3 (n=5) APs with 30 μM R9-CBD3A6K versus 6.7 ± 0.5 (n=5) APs with a vehicle control (*, p <0.05, Student's t-test; Fig. 5B).

3.8. R9-CBD3-A6K suppresses TNI-induced mechanical hypersensitivity

Tibial nerve injury (TNI) induces robust, long-lasting mechanical hypersensitivity indicated by reduction of the tactile threshold in the ipsilateral hindpaw, which was reversed by an acute systemic administration of R9-CBD3A6K (20 mg/kg, intraperitoneal (i.p.)). A single injection of R9-CBD3-A6K produced significant reversal of the tactile threshold towards pre-injury baseline for at least 4 hours; the tactile sensitivity of naïve animals was unaffected by the peptide (Fig. 6A). This duration of reversal of mechanical allodynia is similar to what we observed with TAT-CBD3 [13], TAT-CBD3-A6K [67], or R9-CBD3 [42]. Here, we R9-CBD3-A6K showed an extended duration of action by measuring reversal of mechanical allodynia following drug delivery via subcutaneous (s.c.) osmotic minipumps. Using 24 h minipumps, a 0.17 mg/h (4 mg/day, s.c.) dose started to produce significant anti-allodynic effects starting at 8 h post-initiation of the infusion (Fig. 6C). This effect lasted for about 4 hours after termination of the infusion. Saline infusion did not alter TNI-induced mechanical hypersensitivity (Fig. 6B). Using 72 h minipumps, a 0.22 mg/h (~5.2 mg/day, s.c.) dose elicited a similar time-course of anti-allodynic effects starting at ~10 h post-initiation of the infusion and lasted for 62 h, indicating no tolerance was developed to this effect (Fig. 6D). These results demonstrate that the R9-CBD3-A6K peptide exhibits a long-lasting effect without the development of tolerance within the 72 h continuous infusion. In contrast, opiates such as morphine have been shown to elicit antinociceptive tolerance within 2–3 days [38; 65; 92].

3.9. R9-CBD3A6K induces DA release from NAc in TNI, but not sham, animals

In addition to the efficacy of R9-CBD3A6K in abolishing evoked tactile hypersensitivity, we also examined the release of dopamine (DA) from nucleus accumbens (NAc) shell as a surrogate marker of relief of ongoing pain. Extracellular DA levels in the NAc shell were measured via *in vivo* microdialysis in awake rats. Basal NAc DA levels were not significantly different in sham-operated or tibial nerve-injured (day 14 post-injury) groups with 0.16 ± 0.05 and 0.10 ± 0.02 ng/ml, respectively (P = 0.184, unpaired t-test). We detected a significant increase of DA release in all 6 fractions (total 3 h) after an acute administration of R9-CBD3-A6K (10 mg/kg, i.p.) selectively in rats with nerve injury, consistent with its observed anti-allodynic actions (Fig. 7A). Importantly, the same dose of R9-CBD3-A6K had no effect in sham-operated animals suggesting limited abuse potential. The area under the time effect curve (AUC) also showed significantly higher levels of integrated DA release (Fig. 7B, P < 0.05 TNI/R9-CBD3-A6K vs. TNI/Vehicle or Sham/R9-CBD3-A6K).

3.10. Lack of abuse liability by i.c.v. administration of R9-CBD3-A6K

Potential abuse liability of R9-CBD3A6K was further evaluated using conditioned place preference (CPP) in naïve rats. In order to ensure availability of the peptide to brain reward centers, R9-CBD3A6K was given by the intracerebroventricular (i.c.v.) route and the rats

were paired with a chamber for 5 exposures on consecutive days. The total time spent in the paired chamber was measured 24 hours after the final exposure on day 6, in drug-free animals (Fig. 8). At baseline, all rats spent 43% of the total time in the putative conditioning chamber over a 20-minute period (526.6 seconds; Fig. 8). Unlike our previous studies demonstrating that morphine (i.c.v. dosing) results in a positive condition place preference indicative of the potential of rewarding behavior [48], R9-CBD3-A6K (10 μg in 5 μL, i.c.v.) did not produce a significant increase in total time per chamber (45.7%; p = 0.76) nor a decrease suggesting lack of conditioned place aversion. These data suggest that R9-CBD3-A6K acts neutrally at supraspinal sites and, in the absence of ongoing pain, does not produce rewarding or aversive behaviors.

3.11. Lack of off-target neurobehavioral effects following continuous systemic infusion of R9-CBD3-A6K

A battery of classic behavioral tests was carried out to detect any potential CNS deficits that might induced by chronic administration of R9-CBD3A6K in naïve mice and TNI rats (Fig. 9). Anxiety occurs when there is conflict between risk and reward [50]. The Open-field test (OFT), Light-Dark Box test (LDBT) and the elevated plus maze (EPM) are accepted tests of anxiety-associated behavior that assess the conflict mice have against hiding in enclosed dark areas (i.e., dark box or closed arm) and their tendency to explore novel environments (i.e., white box or open arm) [9; 47]. These tests are also sensitive to anxiolytic drug treatments. Since rodents such as mice and rats display immobile postures when placed in inescapable stressful situations [18; 83], immobility behavior in the tail suspension test (TST) is used as a measure of “depression” or “despair” associated behavior. Furthermore, administering antidepressant treatments prior to testing reduces immobility behavior (see review [23]). Therefore, the TST is often used to screen novel drugs for depressant or anti-depressant properties. Finally, the novel object recognition test is used to evaluate cognition, particularly recognition memory, in rodents [5]. This test is based on the spontaneous tendency of rodents to spend more time exploring a novel object than a familiar one. The choice to explore the novel object reflects the use of learning and recognition memory.

Injecting R9-CBD3-A6K (20 mg/kg, i.p.) 1 hr prior to testing did not alter behaviors in the EPM, and LDBT (Fig. 9A, B) measures of anxiety [50]. In the EPM (n=8,8), there were no differences noted in open arm time/entries ($t_{(14)}$=−1.515, p=0.152/$t_{(14)}$=0.590, p=0.565); closed arm time/entries ($t_{(14)}$=0.495, p=0.628/$t_{(14)}$=1.154, p=0.268); or intersection time/entries ($t_{(14)}$=1.750, p=0.102/$t_{(14)}$=0.648. p=0.527). In the LDBT, neither the latency to enter light compartment ($t_{(13)}$=1.231, p=0.240) nor the percentage of time spent in the light compartment ($t_{(13)}$=1.079, p=0.300) were affected by R9-CBD3-A6K administration (n=7,8, one outlier removed from the vehicle group for being greater than 2 standard deviations away from the mean, Grubb’s test (critical z value = 2.13, p<0.05).

Fig. 9C shows the effect of R9-CBD3-A6K (20 mg/kg, i.p.) at 1 hr post-injection in the TST (n=8,8), where no change in immobility time was noted between treatment groups ($t_{(14)}$= −0.204, p=0.841).

Fig. 9D shows the effect of R9-CBD3-A6K (20 mg/kg, i.p.) at 1 hr post-injection in the NORT (n=8,8), where both vehicle and R9-CBD3-A6K treated animals showed a similar

novelty preference [Object preference $F_{(1,14)}$=10.5, p=0.006; but no treatment $F_{(1,14)}$=0.5, p=0.475, or treatment × object preference noted $F_{(1,14)}$=0.5, p=0.501].

Fig. 9E–F shows the effect of R9-CBD3-A6K (20 mg/kg, i.p.) at 1 hr post-injection in the OFT (n=8,8), where the R9-CBD3-A6K did not alter distance traveled ($t_{(14)}$=0.831, p=0.420), stationary time ($t_{(14)}$= −1.452, p=0.169), time freezing ($t_{(14)}$= −1.444, p=0.171), or inner time ($t_{(14)}$=1.642, p=0.123). R9-CBD3-A6K (~5.2 mg/day, s.c.) also did not alter distance traveled ($F_{(2,6)}$=1.00, p=0.420), stationary duration ($F_{(2,6)}$=3.5, p=0.098), or freezing duration ($F_{(2,6)}$=4.8, p=0.056) when assessed on day 1 (i.e. pre-pump, when the rats exhibited mechanical hypersensitivity (Fig. 6D, *yellow bar*)), day 3 (at 48 h after the start of the minipump, when the mechanical hypersensitivity was completely reversed (Fig. 6D)) and day 4 (at 72 h after the start of the minipump, when the mechanical hypersensitivity was completely reversed (Fig. 6D)) (n=4). These times were chosen for the OFT as the peak of anti-nociception of R9-CBD3-A6K was at 12 h post-infusion with the minipump and remained stable for 60h (until hour 72 when the pump emptied), and likely corresponds to sufficient blood levels of R9-CBD3-A6K to produce anti-nociception. A difference in time spent in inner zone was reduced over time ($F_{(2,6)}$=8.0, p=0.020) for TNI rats. While the reason for this was not investigated further, this is commonly observed when rodents are re-exposed to same arena and it ceases to be novel [40].

4. Discussion

The data reported here demonstrate that R9-CBD3-A6K has pan-Ca^2 interactions that result in reduced calcium influx and excitability of sensory neurons, as well as inhibition of mechanical hypersensitivity and relief of nerve-injury induced ongoing pain. R9-CBD3-A6K was not intrinsically rewarding suggesting a lack of abuse liability and did not promote anxiety or depression or affect learning. Collectively, these data suggest the utility of this novel peptide for treatment of neuropathic pain.

Regulation of voltage-gated calcium channels has been clinically validated as a treatment for neuropathic and other types of pain. CaV2.2 (N-type) channels are highly expressed on nociceptive fibers within the dorsal horn of the spinal cord and essential in relaying pain signals from the periphery to higher centers. Alternative splice variants found on small diameter nociceptive neurons are associated with increased thermal and mechanical hyperalgesia [3; 8]. CaV2.2 is believed to be responsible for increased neurotransmitter release commonly associated with chronic and neuropathic pain conditions [43; 77; 96]. Consistent with the role of CaV2.2 in pain signaling, genetic deletion, as well as pharmacologic block of CaV2.2, impairs nociception [53; 71]. Additionally, central blockade of CaV2.2 is effective in treatment of cases of chronic pain that are intractable to other interventions [11]. Other subtypes of calcium channels, such as CaV2.3 (R-type) [54; 72; 81] or CaV3 (T-type)[35; 51; 58], have also been indicated to play important roles in chronic pain. The CaV2.3-selective blocker, SNX-482, has been reported to block the C- and Aδ- fiber neurotransmission in animal models of chronic neuropathic pain [54] and reduce formalin induced paw-flinching and FOS-expression in the ipsilateral spinal cord [81]. CaV2.3 knockout mice have nociceptive deficits [72]. Low threshold CaV3.2-expressing C fibers have been shown to mediate cold allodynia in humans [74]. Therefore, inhibition of a

broad spectrum of VGCCs by R9-CBD3-A6K may exert synergistic effects among different calcium channel subtypes and underlie its potency and efficacy in ameliorating nerve injury-induced neuropathic pain with improved therapeutic potential when compared to approaches aimed at complete blockade of an individual subtype, especially CaV2.2. Consistent with this possibility, R9-CBD3-A6K did not show any of the side effects associated with Ziconotide [68].

Pain in humans is multidimensional with sensory, affective (aversive) and cognitive components [27]. Preclinical assessment of pain has mainly employed measures of changes in sensory thresholds following induction of an injury [27]. While this approach has been valuable in exploring mechanisms underlying important clinical features of pain including allodynia, capturing affective (i.e., aversive) dimensions of pain that are important to patients in non-verbal animals has been challenging [33; 46; 60]. Our laboratory has evaluated pain motivated behavior and demonstrated that relief of ongoing pain is a natural reward that evokes DA release within the NAc [22; 59], consistent with human imaging studies [6; 7; 24; 62; 93]. We proposed that release of dopamine in the NAc by intrinsically non-rewarding treatments in the setting of injury could represent a translational biomarker of pain relief [24; 62; 69; 93]. In the present study, our data show that R9-CBD3-A6K reverses evoked hypersensitivity in nerve-injured rats. Additionally, R9-CBD3-A6K increased DA release within NAc selectively in injured animals suggesting relief of pain aversiveness and consistent with our previous studies [61; 93]. It seems likely that the effects of R9-CBD3-A6K on both evoked and ongoing pain may result from uncoupling of CRMP2 from calcium channels, limiting calcium influx into neurons to diminish nociceptive input and to activate dopaminergic circuits [4; 78].

It is important to note that R9-CBD3-A6K did not elicit DA release in sham-operated animals, suggesting the enhanced DA efflux in injured animals was due to relief of ongoing pain and not due to an intrinsic rewarding property of R9-CBD3-A6K. Conditioned place preference (CPP), another measure of relief of ongoing pain, was not used here as we have previously reported that there are parallel changes between dopamine release from NAc and the CPP difference score when underlying ongoing pain is present (see reference [93]).

The potential of R9-CBD3-A6K to penetrate into the brain also raises concerns of possible CNS side effects. Intrathecal ω-conotoxin can produce severe CNS side effects such as ataxia and confusion presumably since ω-conotoxin is redistributed to higher centers [2; 82]. However, we did not observe ataxia following R9-CBD3-A6K administration. The lack of CNS side effects was confirmed using a battery of behavioral tests designed to evaluate cognitive and emotional functions, including abuse liability, following acute and chronic R9-CBD3A6K administration. R9-CBD3-A6K did not show any effects in the novel object recognition test suggesting no impact on learning and memory [30; 31]. In addition, the animals spent the same amount of time in the light box (light dark box test) or open arm (elevated plus maze test) after R9-CBD3A6K or vehicle (saline) treatment, suggesting no alterations in the anxiety levels by R9-CBD3A6K administration. Furthermore, there were no distinguishable differences in reaching immobility during the tail suspension test, suggesting no change of depression score after R9-CBD3-A6K administration. Open field test results also showed comparable distance travelled and exploration of the central area by

naïve or nerve-injured rats following 72 h continuous infusion of R9-CBD3-A6K, indicating no disruption of normal locomotion and sensory/motor functions post-sustained R9-CBD3-A6K infusion. We further confirmed lack of abuse liability by five repeated exposures of R9-CBD3-A6K by the intracerebroventricular route to naïve rats using the CPP paradigm. While drugs with intrinsic reward, such as morphine, reliably elicit place conditioning, R9-CBD-3A6K had no effect. This finding suggests a lack of abuse liability and is consistent with the failure of the peptide to elicit NAc DA release in uninjured rats. This is particularly important for new analgesics developed to treat chronic pain on a daily basis in light of the ever rising concerns of prescription drug abuse and overdose [1]. These results confirm a lack of CNS side effects with R9-CBD3-A6K treatment.

Collectively, our data support the conclusion that targeting protein interactions that regulate voltage-gated calcium channels is a promising strategy for pain relief with multiple advantages over direct channel block. Thus, while similar levels of efficacy can be achieved by targeting channel regulation compared to channel function, this approach appears to avoid many of the adverse side effects associated with direct channel block. We have discovered a novel CRMP2 peptide R9-CBD3-A6K that provides excellent efficacy in relieving neuropathic pain. R9-CBD3-A6K does not target specific sensory neuronal subtypes as assessed by constellation pharmacology and produces uniquely long-lasting efficacy. Future studies will use pharmacophore modeling to design small molecule peptidomimetics of CBD3 that may be similarly effective. In conclusion, our results from previous and current studies demonstrate that allosterically targeting CRMP2 interactions with different voltage-gated calcium channel subtypes represents a plausible strategy to ameliorate nerve injury-induced neuropathic pain in humans.

Supplementary Material

Refer to Web version on PubMed Central for supplementary material.

Acknowledgments

This work was supported, in part, by grants from the Indiana Clinical and Translational Sciences Institute funded, in part by a Project Development Team Grant Number (RR025761) from the National Institutes of Health, National Center for Research Resources, Clinical and Translational Sciences Award (F.A.W, P.L.J, R.K), a MERIT Review Award# BX002209 from the U.S. Department of Veterans Affairs, Biomedical Laboratory Research and Development Service (F.A.W.), a NIH DA 034975 grant (F.P.), a National Scientist Development from the American Heart Association (SDG5280023 to R.K.), and a Neurofibromatosis New Investigator Award from the Department of Defense Congressionally Directed Military Medical Research and Development Program (NF1000099 to R.K.).

References

1. United Nations Office on Drugs and Crime. World Drug Report 2015. United Nations publication, Sales No E15XI6
2. Ziconotide: new drug. Limited analgesic efficacy, too many adverse effects. Prescrire international. 2008; 17(97):179–182. [PubMed: 19530373]
3. Altier C, Dale CS, Kisilevsky AE, Chapman K, Castiglioni AJ, Matthews EA, Evans RM, Dickenson AH, Lipscombe D, Vergnolle N, Zamponi GW. Differential role of N-type calcium channel splice isoforms in pain. The Journal of neuroscience : the official journal of the Society for Neuroscience. 2007; 27(24):6363–6373. [PubMed: 17567797]

4. Ansah OB, Leite-Almeida H, Wei H, Pertovaara A. Striatal dopamine D2 receptors attenuate neuropathic hypersensitivity in the rat. Experimental neurology. 2007; 205(2):536–546. [PubMed: 17451685]
5. Antunes M, Biala G. The novel object recognition memory: neurobiology, test procedure, and its modifications. Cogn Process. 2012; 13(2):93–110. [PubMed: 22160349]
6. Baliki MN, Geha PY, Fields HL, Apkarian AV. Predicting value of pain and analgesia: nucleus accumbens response to noxious stimuli changes in the presence of chronic pain. Neuron. 2010; 66(1):149–160. [PubMed: 20399736]
7. Becerra L, Navratilova E, Porreca F, Borsook D. Analogous responses in the nucleus accumbens and cingulate cortex to pain onset (aversion) and offset (relief) in rats and humans. J Neurophysiol. 2013; 110(5):1221–1226. [PubMed: 23785130]
8. Bell TJ, Thaler C, Castiglioni AJ, Helton TD, Lipscombe D. Cell-specific alternative splicing increases calcium channel current density in the pain pathway. Neuron. 2004; 41(1):127–138. [PubMed: 14715140]
9. Bourin M, Hascoet M. The mouse light/dark box test. Eur J Pharmacol. 2003; 463(1–3):55–65. [PubMed: 12600702]
10. Bourinet E, Zamponi GW. Voltage gated calcium channels as targets for analgesics. Current topics in medicinal chemistry. 2005; 5(6):539–546. [PubMed: 16022676]
11. Bowersox SS, Singh T, Nadasdi L, Zukowska-Grojec Z, Valentino K, Hoffman BB. Cardiovascular effects of omega-conopeptides in conscious rats: mechanisms of action. J Cardiovasc Pharmacol. 1992; 20(5):756–764. [PubMed: 1280738]
12. Brittain JM, Chen L, Wilson SM, Brustovetsky T, Gao X, Ashpole NM, Molosh AI, You H, Hudmon A, Shekhar A, White FA, Zamponi GW, Brustovetsky N, Chen J, Khanna R. Neuroprotection against traumatic brain injury by a peptide derived from the collapsin response mediator protein 2 (CRMP2). The Journal of biological chemistry. 2011; 286(43):37778–37792. [PubMed: 21832084]
13. Brittain JM, Duarte DB, Wilson SM, Zhu W, Ballard C, Johnson PL, Liu N, Xiong W, Ripsch MS, Wang Y, Fehrenbacher JC, Fitz SD, Khanna M, Park CK, Schmutzler BS, Cheon BM, Due MR, Brustovetsky T, Ashpole NM, Hudmon A, Meroueh SO, Hingtgen CM, Brustovetsky N, Ji RR, Hurley JH, Jin X, Shekhar A, Xu XM, Oxford GS, Vasko MR, White FA, Khanna R. Suppression of inflammatory and neuropathic pain by uncoupling CRMP-2 from the presynaptic Ca(2)(+) channel complex. Nature medicine. 2011; 17(7):822–829.
14. Brittain JM, Piekarz AD, Wang Y, Kondo T, Cummins TR, Khanna R. An atypical role for collapsin response mediator protein 2 (CRMP-2) in neurotransmitter release via interaction with presynaptic voltage-gated calcium channels. The Journal of biological chemistry. 2009; 284(45): 31375–31390. [PubMed: 19755421]
15. Cao YQ. Voltage-gated calcium channels and pain. Pain. 2006; 126(1–3):5–9. [PubMed: 17084979]
16. Caterina MJ, Julius D. The vanilloid receptor: a molecular gateway to the pain pathway. Annual review of neuroscience. 2001; 24:487–517.
17. Chaplan SR, Bach FW, Pogrel JW, Chung JM, Yaksh TL. Quantitative assessment of tactile allodynia in the rat paw. J Neurosci Methods. 1994; 53(1):55–63. [PubMed: 7990513]
18. Chermat R, Thierry B, Mico JA, Steru L, Simon P. Adaptation of the tail suspension test to the rat. J Pharmacol. 1986; 17(3):348–350. [PubMed: 3795979]
19. Chi XX, Schmutzler BS, Brittain JM, Hingtgen CM, Nicol GD, Khanna R. Regulation of N-type voltage-gated calcium (CaV2.2) channels and transmitter release by collapsin response mediator protein-2 (CRMP-2) in sensory neurons. J Cell Sci. 2009; 23:4351–4362. [PubMed: 19903690]
20. Choe W, Messinger RB, Leach E, Eckle VS, Obradovic A, Salajegheh R, Jevtovic-Todorovic V, Todorovic SM. TTA-P2 is a potent and selective blocker of T-type calcium channels in rat sensory neurons and a novel antinociceptive agent. Mol Pharmacol. 2011; 80(5):900–910. [PubMed: 21821734]
21. Cizkova D, Marsala J, Lukacova N, Marsala M, Jergova S, Orendacova J, Yaksh TL. Localization of N-type Ca2+ channels in the rat spinal cord following chronic constrictive nerve injury. Exp Brain Res. 2002; 147(4):456–463. [PubMed: 12444477]

22. Craig AD. Interoception: the sense of the physiological condition of the body. Curr Opin Neurobiol. 2003; 13(4):500–505. [PubMed: 12965300]
23. Cryan JF, Mombereau C, Vassout A. The tail suspension test as a model for assessing antidepressant activity: review of pharmacological and genetic studies in mice. Neurosci Biobehav Rev. 2005; 29(4–5):571–625. [PubMed: 15890404]
24. De Felice M, Eyde N, Dodick D, Dussor GO, Ossipov MH, Fields HL, Porreca F. Capturing the aversive state of cephalic pain preclinically. Annals of neurology. 2013
25. Dogrul A, Gardell LR, Ossipov MH, Tulunay FC, Lai J, Porreca F. Reversal of experimental neuropathic pain by T-type calcium channel blockers. Pain. 2003; 105(1–2):159–168. [PubMed: 14499432]
26. Feng ZP, Hamid J, Doering C, Bosey GM, Snutch TP, Zamponi GW. Residue Gly1326 of the N-type calcium channel alpha 1B subunit controls reversibility of omega-conotoxin GVIA and MVIIA block. The Journal of biological chemistry. 2001; 276(19):15728–15735. [PubMed: 11279062]
27. Fields HL. Pain: an unpleasant topic. Pain. 1999; (Suppl 6):S61–69. [PubMed: 10491974]
28. Fischer G, Pan B, Vilceanu D, Hogan QH, Yu H. Sustained relief of neuropathic pain by AAV-targeted expression of CBD3 peptide in rat dorsal root ganglion. Gene therapy. 2014; 21(1):44–51. [PubMed: 24152582]
29. Francois-Moutal L, Wang Y, Moutal A, Cottier KE, Melemedjian OK, Yang X, Wang Y, Ju W, Largent-Milnes TM, Khanna M, Vanderah TW, Khanna R. A membrane-delimited N-myristoylated CRMP2 peptide aptamer inhibits CaV2.2 trafficking and reverses inflammatory and postoperative pain behaviors. Pain. 2015; 156(7):1247–1264. [PubMed: 25782368]
30. Gao XM, Elmer GI, Adams-Huet B, Tamminga CA. Social memory in mice: disruption with an NMDA antagonist and attenuation with antipsychotic drugs. Pharmacol Biochem Behav. 2009; 92(2):236–242. [PubMed: 19103218]
31. Gould TJ, McCarthy MM, Keith RA. MK-801 disrupts acquisition of contextual fear conditioning but enhances memory consolidation of cued fear conditioning. Behav Pharmacol. 2002; 13(4): 287–294. [PubMed: 12218509]
32. Greffrath W, Kirschstein T, Nawrath H, Treede R. Changes in cytosolic calcium in response to noxious heat and their relationship to vanilloid receptors in rat dorsal root ganglion neurons. Neuroscience. 2001; 104(2):539–550. [PubMed: 11377853]
33. Gregory NS, Harris AL, Robinson CR, Dougherty PM, Fuchs PN, Sluka KA. An overview of animal models of pain: disease models and outcome measures. J Pain. 2013; 14(11):1255–1269. [PubMed: 24035349]
34. Heblich F, Tran Van Minh A, Hendrich J, Watschinger K, Dolphin AC. Time course and specificity of the pharmacological disruption of the trafficking of voltage-gated calcium channels by gabapentin. Channels (Austin). 2008; 2(1):4–9. [PubMed: 18690052]
35. Hildebrand ME, Smith PL, Bladen C, Eduljee C, Xie JY, Chen L, Fee-Maki M, Doering CJ, Mezeyova J, Zhu Y, Belardetti F, Pajouhesh H, Parker D, Arneric SP, Parmar M, Porreca F, Tringham E, Zamponi GW, Snutch TP. A novel slow-inactivation-specific ion channel modulator attenuates neuropathic pain. Pain. 2011; 152(4):833–843. [PubMed: 21349638]
36. Himmel HM, Kiss T, Borvendeg SJ, Gillen C, Illes P. The arginine-rich hexapeptide R4W2 is a stereoselective antagonist at the vanilloid receptor 1: a Ca2+ imaging study in adult rat dorsal root ganglion neurons. The Journal of pharmacology and experimental therapeutics. 2002; 301(3):981–986. [PubMed: 12023528]
37. Hubbard KE, Wells A, Owens TS, Tagen M, Fraga CH, Stewart CF. Determination of dopamine, serotonin, and their metabolites in pediatric cerebrospinal fluid by isocratic high performance liquid chromatography coupled with electrochemical detection. Biomed Chromatogr. 2010; 24(6): 626–631. [PubMed: 19810006]
38. Ingram SL, Fossum EN, Morgan MM. Behavioral and electrophysiological evidence for opioid tolerance in adolescent rats. Neuropsychopharmacology. 2007; 32(3):600–606. [PubMed: 16823389]
39. Jagodic MM, Pathirathna S, Nelson MT, Mancuso S, Joksovic PM, Rosenberg ER, Bayliss DA, Jevtovic-Todorovic V, Todorovic SM. Cell-specific alterations of T-type calcium current in painful

diabetic neuropathy enhance excitability of sensory neurons. J Neurosci. 2007; 27(12):3305–3316. [PubMed: 17376991]

40. Johnson PL, Federici LM, Fitz SD, Renger JJ, Shireman B, Winrow CJ, Bonaventure P, Shekhar A. Orexin 1 and 2 Receptor Involvement in Co2 -Induced Panic-Associated Behavior and Autonomic Responses. Depress Anxiety. 2015; 32(9):671–683. [PubMed: 26332431]
41. Joiner WJ, Khanna R, Schlichter LC, Kaczmarek LK. Calmodulin regulates assembly and trafficking of SK4/IK1 Ca2+-activated K+ channels. The Journal of biological chemistry. 2001; 276(41):37980–37985. [PubMed: 11495911]
42. Ju W, Li Q, Allette YM, Ripsch MS, White FA, Khanna R. Suppression of pain-related behavior in two distinct rodent models of peripheral neuropathy by a homopolyarginine-conjugated CRMP2 peptide. Journal of neurochemistry. 2012; 124(6):869–879. [PubMed: 23106100]
43. Kerr LM, Filloux F, Olivera BM, Jackson H, Wamsley JK. Autoradiographic localization of calcium channels with [125I]omega-conotoxin in rat brain. Eur J Pharmacol. 1988; 146(1):181–183. [PubMed: 2450766]
44. Khanna R, Wilson SM, Brittain JM, Weimer JM, Sultana R, Butterfield AD, Hensley K. Opening Pandoras' jar: a primer on the putative roles of CRMP2 in a panoply of neurodegenerative, sensory and motor neurons, and central disorders. Future Neurol. 2012; 5(5):749–771. [PubMed: 23308041]
45. Kilkenny C, Browne WJ, Cuthill IC, Emerson M, Altman DG. Improving bioscience research reporting: The ARRIVE guidelines for reporting animal research. J Pharmacol Pharmacother. 2010; 1(2):94–99. [PubMed: 21350617]
46. King T, Vera-Portocarrero L, Gutierrez T, Vanderah TW, Dussor G, Lai J, Fields HL, Porreca F. Unmasking the tonic-aversive state in neuropathic pain. Nat Neurosci. 2009; 12(11):1364–1366. [PubMed: 19783992]
47. Lalonde R, Strazielle C. Relations between open-field, elevated plus-maze, and emergence tests as displayed by C57/BL6J and BALB/c mice. J Neurosci Methods. 2008; 171(1):48–52. [PubMed: 18358538]
48. Largent-Milnes TM, Brookshire SW, Skinner DP Jr, Hanlon KE, Giuvelis D, Yamamoto T, Davis P, Campos CR, Nair P, Deekonda S, Bilsky EJ, Porreca F, Hruby VJ, Vanderah TW. Building a better analgesic: multifunctional compounds that address injury-induced pathology to enhance analgesic efficacy while eliminating unwanted side effects. The Journal of pharmacology and experimental therapeutics. 2013; 347(1):7–19. [PubMed: 23860305]
49. Lee MS. Recent progress in the discovery and development of N-type calcium channel modulators for the treatment of pain. Prog Med Chem. 2014; 53:147–186. [PubMed: 24418610]
50. Lowry CA, Johnson PL, Hay-Schmidt A, Mikkelsen J, Shekhar A. Modulation of anxiety circuits by serotonergic systems. Stress. 2005; 8(4):233–246. [PubMed: 16423712]
51. M'Dahoma S, Gadotti VM, Zhang FX, Park B, Nam JH, Onnis V, Balboni G, Lee JY, Zamponi GW. Effect of the T-type channel blocker KYS-05090S in mouse models of acute and neuropathic pain. Pflugers Arch. 2015
52. Ma C, Shu Y, Zheng Z, Chen Y, Yao H, Greenquist KW, White FA, LaMotte RH. Similar electrophysiological changes in axotomized and neighboring intact dorsal root ganglion neurons. J Neurophysiol. 2003; 89(3):1588–1602. [PubMed: 12612024]
53. Malmberg AB, Yaksh TL. Voltage-sensitive calcium channels in spinal nociceptive processing: blockade of N- and P-type channels inhibits formalin-induced nociception. J Neurosci. 1994; 14(8):4882–4890. [PubMed: 8046458]
54. Matthews EA, Bee LA, Stephens GJ, Dickenson AH. The Cav2.3 calcium channel antagonist SNX-482 reduces dorsal horn neuronal responses in a rat model of chronic neuropathic pain. The European journal of neuroscience. 2007; 25(12):3561–3569. [PubMed: 17610575]
55. Metz AE, Jarsky T, Martina M, Spruston N. R-type calcium channels contribute to afterdepolarization and bursting in hippocampal CA1 pyramidal neurons. J Neurosci. 2005; 25(24):5763–5773. [PubMed: 15958743]
56. Mintz IM, Venema VJ, Swiderek KM, Lee TD, Bean BP, Adams ME. P-type calcium channels blocked by the spider toxin omega-Aga-IVA. Nature. 1992; 355(6363):827–829. [PubMed: 1311418]

57. Moutal A, Chew LA, Yang X, Wang Y, Yeon SK, Telemi E, Meroueh S, Park KD, Shrinivasan R, Gilbraith KB, Qu C, Xie JY, Patwardhan A, Vanderah TW, Khanna M, Porreca F, Khanna R. (S)-Lacosamide inhibition of CRMP2 phosphorylation reduces postoperative and neuropathic pain behaviors through distinct classes of sensory neurons identified by constellation pharmacology. Pain. 2016
58. Murakami-Nakayama M, Tsubota M, Hiruma S, Sekiguchi F, Matsuyama K, Kimura T, Moriyama M, Kawabata A. Polaprezinc attenuates cyclophosphamide-induced cystitis and related bladder pain in mice. J Pharmacol Sci. 2015; 127(2):223–228. [PubMed: 25727961]
59. Murray, EA.; Wise, SP.; Rhodes, SEV. What Can Different Brains Do with Reward?. In: Gottfried, JA., editor. Neurobiology of Sensation and Reward. Boca Raton (FL): 2011.
60. Navratilova E, Xie JY, King T, Porreca F. Evaluation of reward from pain relief. Ann N Y Acad Sci. 2013; 1282:1–11. [PubMed: 23496247]
61. Navratilova E, Xie JY, Okun A, Qu C, Eyde N, Ci S, Ossipov MH, King T, Fields HL, Porreca F. Pain relief produces negative reinforcement through activation of mesolimbic reward-valuation circuitry. Proceedings of the National Academy of Sciences of the United States of America. 2012; 109(50):20709–20713. [PubMed: 23184995]
62. Navratilova E, Xie JY, Okun A, Qu C, Eyde N, Ci S, Ossipov MH, King T, Fields HL, Porreca F. Pain relief produces negative reinforcement through activation of mesolimbic reward-valuation circuitry. Proc Natl Acad Sci U S A. 2012; 109(50):20709–20713. [PubMed: 23184995]
63. Newcomb R, Szoke B, Palma A, Wang G, Chen X, Hopkins W, Cong R, Miller J, Urge L, Tarczy-Hornoch K, Loo JA, Dooley DJ, Nadasdi L, Tsien RW, Lemos J, Miljanich G. Selective peptide antagonist of the class E calcium channel from the venom of the tarantula Hysterocrates gigas. Biochemistry. 1998; 37(44):15353–15362. [PubMed: 9799496]
64. Okun A, Liu P, Davis P, Ren J, Remeniuk B, Brion T, Ossipov MH, Xie J, Dussor GO, King T, Porreca F. Afferent drive elicits ongoing pain in a model of advanced osteoarthritis. Pain. 2012; 153(4):924–933. [PubMed: 22387095]
65. Ozdemir E, Gursoy S, Bagcivan I, Durmus N, Altun A. Zimelidine attenuates the development of tolerance to morphine-induced antinociception. Indian J Pharmacol. 2012; 44(2):215–218. [PubMed: 22529478]
66. Park J, Luo ZD. Calcium channel functions in pain processing. Channels (Austin). 2010; 4(6):510–517. [PubMed: 21150297]
67. Piekarz AD, Due MR, Khanna M, Wang B, Ripsch MS, Wang R, Meroueh SO, Vasko MR, White FA, Khanna R. CRMP-2 peptide mediated decrease of high and low voltage-activated calcium channels, attenuation of nociceptor excitability, and anti-nociception in a model of AIDS therapy-induced painful peripheral neuropathy. Molecular pain. 2012; 8(1):54. [PubMed: 22828369]
68. Rauck RL, Wallace MS, Burton AW, Kapural L, North JM. Intrathecal ziconotide for neuropathic pain: a review. Pain practice : the official journal of World Institute of Pain. 2009; 9(5):327–337. [PubMed: 19682321]
69. Remeniuk B, Sukhtankar D, Okun A, Navratilova E, Xie JY, King T, Porreca F. Behavioral and neurochemical analysis of ongoing bone cancer pain in rats. Pain. 2015; 156(10):1864–1873. [PubMed: 25955964]
70. Ripsch MS, Ballard CJ, Khanna M, Hurley JH, White FA, Khanna R. A PEPTIDE UNCOUPLING CRMP-2 FROM THE PRESYNAPTIC Ca(2+) CHANNEL COMPLEX DEMONSTRATES EFFICACY IN ANIMAL MODELS OF MIGRAINE AND AIDS THERAPY-INDUCED NEUROPATHY. Translational neuroscience. 2012; 3(1):1–8. [PubMed: 22662308]
71. Saegusa H, Kurihara T, Zong S, Kazuno A, Matsuda Y, Nonaka T, Han W, Toriyama H, Tanabe T. Suppression of inflammatory and neuropathic pain symptoms in mice lacking the N-type Ca2+ channel. EMBO J. 2001; 20(10):2349–2356. [PubMed: 11350923]
72. Saegusa H, Kurihara T, Zong S, Minowa O, Kazuno A, Han W, Matsuda Y, Yamanaka H, Osanai M, Noda T, Tanabe T. Altered pain responses in mice lacking alpha 1E subunit of the voltage-dependent Ca2+ channel. Proc Natl Acad Sci U S A. 2000; 97(11):6132–6137. [PubMed: 10801976]
73. Saegusa H, Matsuda Y, Tanabe T. Effects of ablation of N- and R-type Ca(2+) channels on pain transmission. Neurosci Res. 2002; 43(1):1–7. [PubMed: 12074836]

74. Samour MS, Nagi SS, Mahns DA. Cav3.2-expressing low-threshold C fibres in human hairy skin contribute to cold allodynia–a non-TRPV1- and non-TRPM8-dependent phenomenon. Pain. 2015; 156(8):1566–1575. [PubMed: 25932689]
75. Schmidtko A, Lotsch J, Freynhagen R, Geisslinger G. Ziconotide for treatment of severe chronic pain. Lancet. 2010; 375(9725):1569–1577. [PubMed: 20413151]
76. Skov MJ, Beck JC, de Kater AW, Shopp GM. Nonclinical safety of ziconotide: an intrathecal analgesic of a new pharmaceutical class. International journal of toxicology. 2007; 26(5):411–421. [PubMed: 17963128]
77. Snutch TP. Targeting chronic and neuropathic pain: the N-type calcium channel comes of age. Neuro Rx. 2005; 2(4):662–670.
78. Taylor BK, Joshi C, Uppal H. Stimulation of dopamine D2 receptors in the nucleus accumbens inhibits inflammatory pain. Brain research. 2003; 987(2):135–143. [PubMed: 14499957]
79. Teichert RW, Memon T, Aman JW, Olivera BM. Using constellation pharmacology to define comprehensively a somatosensory neuronal subclass. Proc Natl Acad Sci U S A. 2014; 111(6): 2319–2324. [PubMed: 24469798]
80. Teichert RW, Schmidt EW, Olivera BM. Constellation pharmacology: a new paradigm for drug discovery. Annu Rev Pharmacol Toxicol. 2015; 55:573–589. [PubMed: 25562646]
81. Terashima T, Xu Q, Yamaguchi S, Yaksh TL. Intrathecal P/Q- and R-type calcium channel blockade of spinal substance P release and c-Fos expression. Neuropharmacology. 2013; 75:1–8. [PubMed: 23810829]
82. Thompson JC, Dunbar E, Laye RR. Treatment challenges and complications with ziconotide monotherapy in established pump patients. Pain physician. 2006; 9(2):147–152. [PubMed: 16703976]
83. Varty GB, Cohen-Williams ME, Hunter JC. The antidepressant-like effects of neurokinin NK1 receptor antagonists in a gerbil tail suspension test. Behav Pharmacol. 2003; 14(1):87–95. [PubMed: 12576885]
84. Wallace MS. Ziconotide: a new nonopioid intrathecal analgesic for the treatment of chronic pain. Expert review of neurotherapeutics. 2006; 6(10):1423–1428. [PubMed: 17078783]
85. Wang Y, Brittain JM, Jarecki BW, Park KD, Wilson SM, Wang B, Hale R, Meroueh SO, Cummins TR, Khanna R. In silico docking and electrophysiological characterization of lacosamide binding sites on collapsin response mediator protein-2 identifies a pocket important in modulating sodium channel slow inactivation. The Journal of biological chemistry. 2010; 285(33):25296–25307. [PubMed: 20538611]
86. Wang Y, Brittain JM, Wilson SM, Khanna R. Emerging roles of collapsin response mediator proteins (CRMPs) as regulators of voltage-gated calcium channels and synaptic transmission. Communicative & Integrative Biology. 2010; 3(2):1–4. [PubMed: 20539772]
87. Wender PA, Mitchell DJ, Pattabiraman K, Pelkey ET, Steinman L, Rothbard JB. The design, synthesis, and evaluation of molecules that enable or enhance cellular uptake: peptoid molecular transporters. Proc Natl Acad Sci USA. 2000; 97(24):13003–13008. [PubMed: 11087855]
88. Wheeler DG, Groth RD, Ma H, Barrett CF, Owen SF, Safa P, Tsien RW. Ca(V)1 and Ca(V)2 channels engage distinct modes of Ca(2+) signaling to control CREB-dependent gene expression. Cell. 2012; 149(5):1112–1124. [PubMed: 22632974]
89. Wilson SM, Brittain JM, Piekarz AD, Ballard CJ, Ripsch MS, Cummins TR, Hurley JH, Khanna M, Hammes NM, Samuels BC, White FA, Khanna R. Further insights into the antinociceptive potential of a peptide disrupting the N-type calcium channel-CRMP-2 signaling complex. Channels (Austin). 2011; 5(5):449–456. [PubMed: 21829088]
90. Wilson SM, Schmutzler BS, Brittain JM, Dustrude ET, Ripsch MS, Pellman JJ, Yeum TS, Hurley JH, Hingtgen CM, White FA, Khanna R. Inhibition of Transmitter Release and Attenuation of AIDS Therapy-Induced and Tibial Nerve Injury-Related Painful Peripheral Neuropathy by Novel Synthetic Ca2+ Channel Peptides. The Journal of biological chemistry. 2012; 287(42):35065–35077. [PubMed: 22891239]
91. Winter J, Dray A, Wood JN, Yeats JC, Bevan S. Cellular mechanism of action of resiniferatoxin: a potent sensory neuron excitotoxin. Brain research. 1990; 520(1–2):131–140. [PubMed: 2169951]

92. Wong CS, Hsu MM, Chou R, Chou YY, Tung CS. Intrathecal cyclooxygenase inhibitor administration attenuates morphine antinociceptive tolerance in rats. Br J Anaesth. 2000; 85(5): 747–751. [PubMed: 11094592]

93. Xie JY, Qu C, Patwardhan A, Ossipov MH, Navratilova E, Becerra L, Borsook D, Porreca F. Activation of mesocorticolimbic reward circuits for assessment of relief of ongoing pain: a potential biomarker of efficacy. Pain. 2014; 155(8):1659–1666. [PubMed: 24861580]

94. Zamponi GW. Welcome to “ion channels: key therapeutic targets”. Future medicinal chemistry. 2010; 2(5):689–690. [PubMed: 21426195]

95. Zamponi GW. Targeting voltage-gated calcium channels in neurological and psychiatric diseases. Nature reviews Drug discovery. 2016; 15(1):19–34. [PubMed: 26542451]

96. Zamponi GW, Lewis RJ, Todorovic SM, Arneric SP, Snutch TP. Role of voltage-gated calcium channels in ascending pain pathways. Brain research reviews. 2009; 60(1):84–89. [PubMed: 19162069]

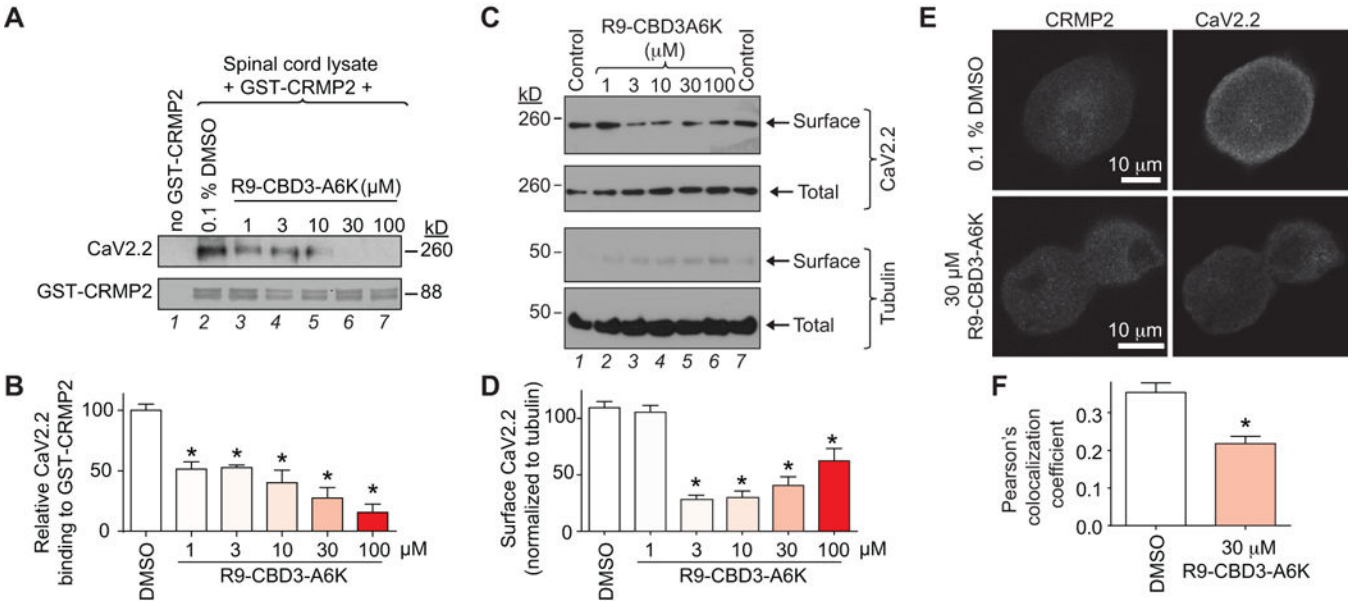

Figure 1. R9-CBD3-A6K peptide inhibits the CaV2.2–CRMP2 interaction to decrease surface CaV2.2

(**A**) Spinal cord lysates were incubated with recombinant CRMP2-GST protein (0.4 μM) in the absence (0.1% DMSO, *lane 2*) or presence of increasing concentrations (as indicated) of peptide. The CRMP2-GST bound proteins were recovered by incubation with glutathione sepharose beads and immunoblotted with CaV2.2 (*top*) and CRMP2 (*bottom*). Representative blots from 3 separate experiments are shown. (**B**) Summary of mean relative binding of CaV2.2 to CRMP2. CaV2.2-CRMP2 binding was reduced by R9-CBD3-A6K in a concentration-dependent manner (*, $p < 0.01$; one-way ANOVA with Tukey's post-hoc test). $n = 3$ separate, individual experiments. (**C**) Cell–surface expression of CaV2.2 was monitored using a biotinylation assay. Acutely isolated DRGs cells, incubated with no peptide (control) or increasing amounts of R9-CBD3-A6K peptide, were biotinylated, the cell-surface proteins were harvested from the cell lysates, and the precipitates were analyzed by immunoblotting with CaV2.2 (*top 2 blots*) and βIII-tubulin (*bottom 2 blots*) antibodies. Equal amounts of samples were used for the precipitation of biotinylated proteins. Of these samples, the entire biotinylated fraction (surface) and 10% of the non-biotinylated (total) fraction were loaded. R9-CBD3-A6K decreased the amount of CaV2.2 at the cell surface compared to peptide-treated neurons. No change was observed in the total levels of CaV2.2 or tubulin. Representative blots of surface biotinylated and total fractions immunoblotted with a CaV2.2 antibody (*top*) or tubulin (*bottom*) are shown ($n = 3$ separate, individual experiments). (**D**) Averaged CaV2.2 surface expression, normalized to total CaV2.2 and then to total tubulin (*, $p < 0.05$; one-way ANOVA with Tukey's post-hoc test). (**E**) Representative micrographs of DRG cells immunolabeled with CRMP2 and CaV2.2. The neurons are treated with 0.1% DMSO or with R9-CBD3-A6K (30 μM) for 48 hrs. Control cells not treated with the peptide display an overlap in membrane labeling of both CaV2.2 and CRMP2. At 48 hrs CaV2.2 and CRMP2 labeling is scattered in distinct puncta within the cytosol. Scale bar length is 10 μm. (**F**) Quantification of colocalization of CaV2.2 with CRMP2 was carried using Pearson's overlap method. The values in the graph are the overlap

coefficients. $n = 2$ separate, individual experiments; the total number of cells analyzed is 14–17 per condition.

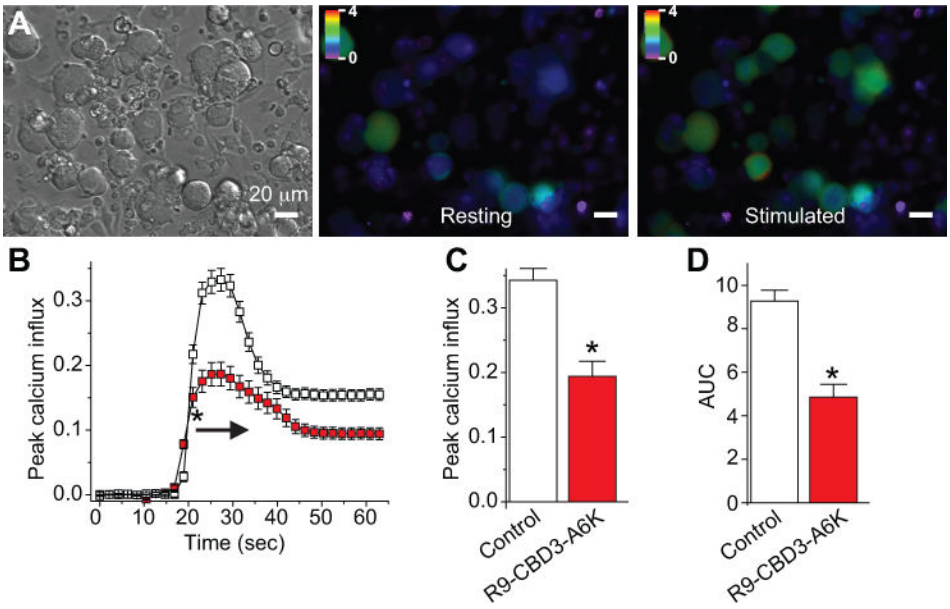

Figure 2. R9-CBD3-A6K inhibits K^+-stimulated Ca^{2+} influx in DRG neurons

Differential interference contrast (DIC) and pseudocolored fluorescent images of a field of DRG neurons visualized for Fura-2, before and after stimulation with KCl (**A**). Ca^{2+} imaging was performed on adult rat DRG neurons using the ratiometric Ca^{2+}-sensitive dye Fura-2. Following a 1 min baseline measurement, neurons were stimulated with 90 mM KCl for 30–40 sec to induce Ca^{2+} influx. (**B**) Line graph shows the peak calcium influx (fluorescence response adjusted for background) over time of DRGs incubated for 20 min with 30 μM R9-CBD3-A6K was reduced to about 40% of that of untreated DRGs. Peak calcium influx (**C**) and integrated area under curve (AUC, **D**) also shows significant reduction of the calcium influx with pretreatment of R9-CBD3-A6K ((*, p <0.01; Student's t-test). Values represent the average ± SEM from three separate imaging experiments from >100 cells per condition.

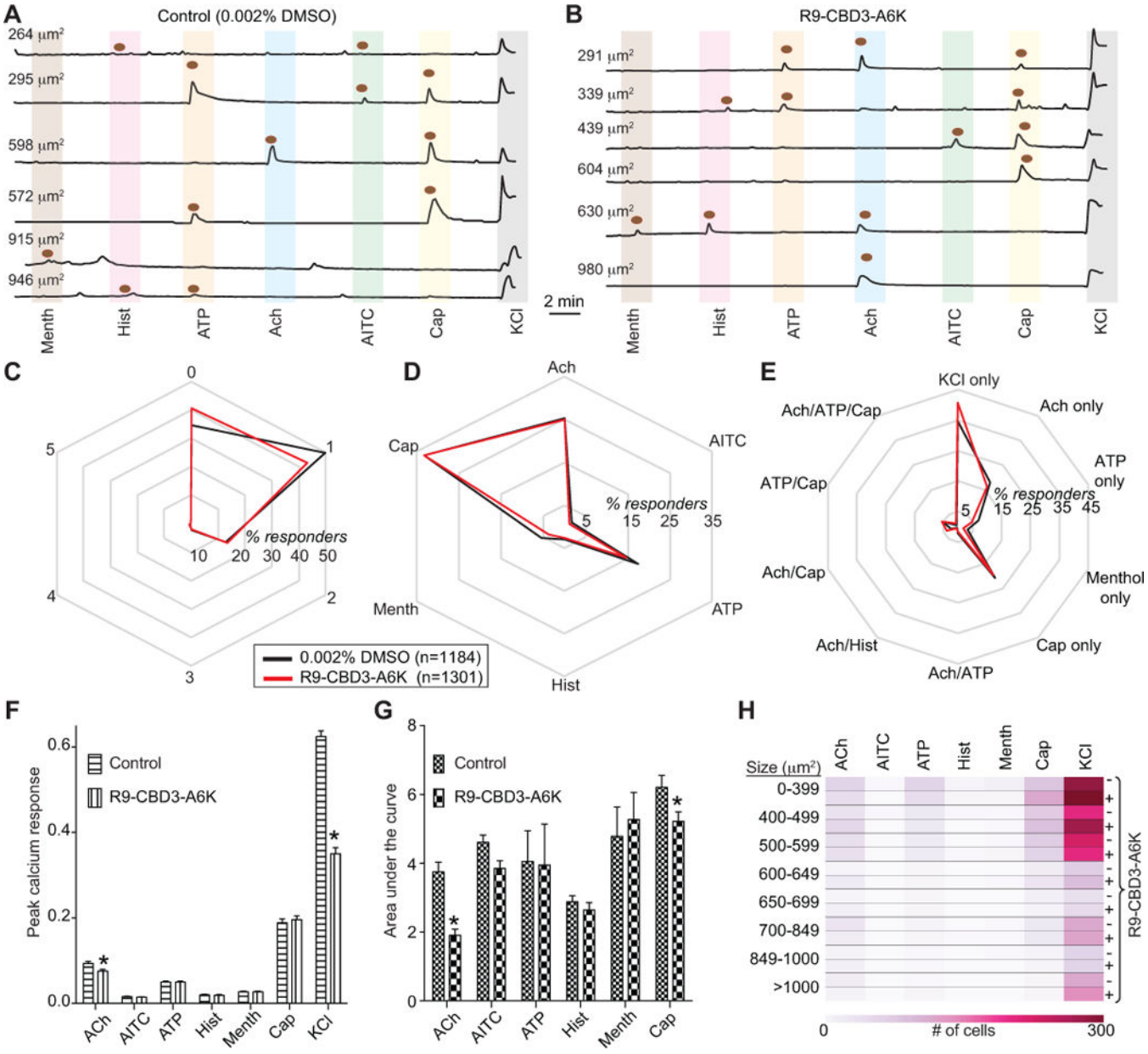

Figure 3. Functional 'fingerprinting' of DRG neuronal subclasses following treatment with R9-CBD3-A6K

(**A**) Ca^{2+}-imaging traces of DRGs responding to constellation pharmacology agonist or membrane-potential triggers. Each trace represents the response of a different neuron. In a typical experimental trial, the responses (*filled brown circles*) of >100 individual neurons were monitored simultaneously. Selected traces are shown. The abbreviations used are defined in Table 1. Colored columns indicate the ~15-s application of challenge compounds or high [K+]o; after each application the free compound or high [K+]o was continuously washed out of the well with room-temperature bath solution. The y-axis shows the Fura-2AM fluorescence ratio (F_{340}/F_{380}) for each trace. Raw, unfiltered traces are presented. Triggers used were: menthol (400 nM), histamine (50 µM), ATP (10 µM), AITC (200 µM), acetylcholine (1 mM), capsaicin (100 nM) and KCl (90 mM). DRG neurons were treated

with either vehicle (0.002% DMSO) (**A**) or R9-CBD3-A6K (**B**) and the neuronal populations analyzed by the constellation pharmacology protocol. All cells were selected based on their response to the depolarizing pulse of KCl. Size of each cell is indicated by the surface area value in each trace. (**C**) The response of DRG neurons to one or more constellation pharmacology trigger was analyzed. The polar plot indicates the percentage of cells that responded to the indicated number of triggers independently of which compound they responded to. The number 0 corresponds to the proportion of cells that responded to KCl only and no other trigger. No significant change was observed in each category of cells after treatment with (*S*)-LCM. (**D**) Polar plot showing the percent of cells responding to each constellation pharmacology trigger independently of any other trigger that the cell also responded to. Each axis shows a different trigger. (**E**) Polar plot showing the percent of cells responding to major classes of triggers. Data are from 3 independent experiments with a total n=1184 for control and n=1301 for 10μM R9-CBD3-A6K. (**F**) Bar graph showing the average peak (**F**) or area under the curve (AUC) (**G**) calcium response in the major functional neuronal populations identified in (**D**). AUC was calculated with Prism software using the trapezoid rule. R9-CBD3-A6K did not decrease the peak calcium influx in response to any trigger except Ach and KCl for peak or Ach and Cap for and AUC (*, $p<0.05$; Student's t-test). An AUC for KCl was not calculated in these experiments since KCl was the last trigger (see traces in **A** and **B**). (**H**) Heatmap of the size distribution of neurons responsive to the conditions show in **D**.

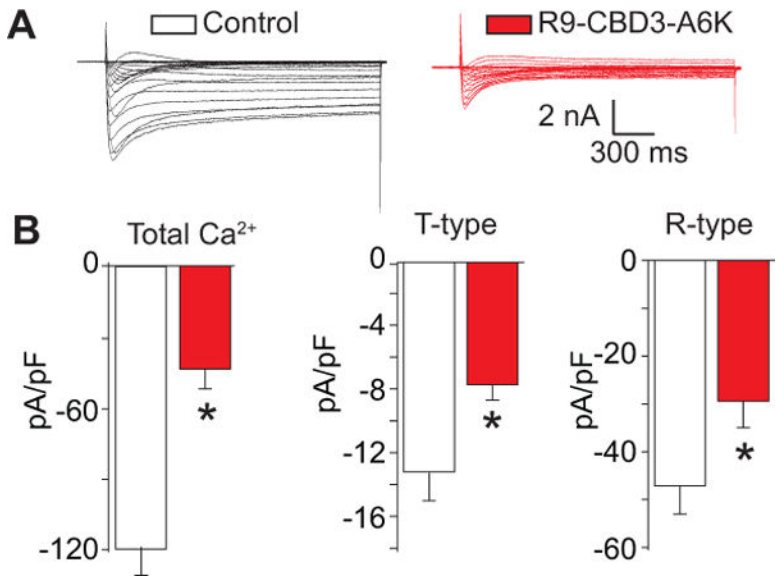

Figure 4. Acute application of R9-CBD3-A6K decreases Ca^{2+} currents in sensory neurons

(**A**) Representative family of current traces are illustrated for control- (0.002% DMSO) or 10 μM R9-CBD3-A6K-treated neurons. Currents were evoked by 200 millisecond prepulses between −90 mV and +60 mV. (**B**) Summary of the peak current density (pA/pF) from sensory neurons in the absence or presence of 10 μM R9-CBD3-A6K for total (*left*), T-type (*middle*), and R-type (*right*) Ca^{2+} currents. Calcium channel subtypes were isolated using pharmacological blockers and appropriate voltage protocols, as described previously [67]. n=11–18 cells for control and n=12–19 cells for 10 μM R9-CBD3-A6K-treated cells; asterisk indicates statistical significance compared with control cells ($p<0.05$, Student's t-test).

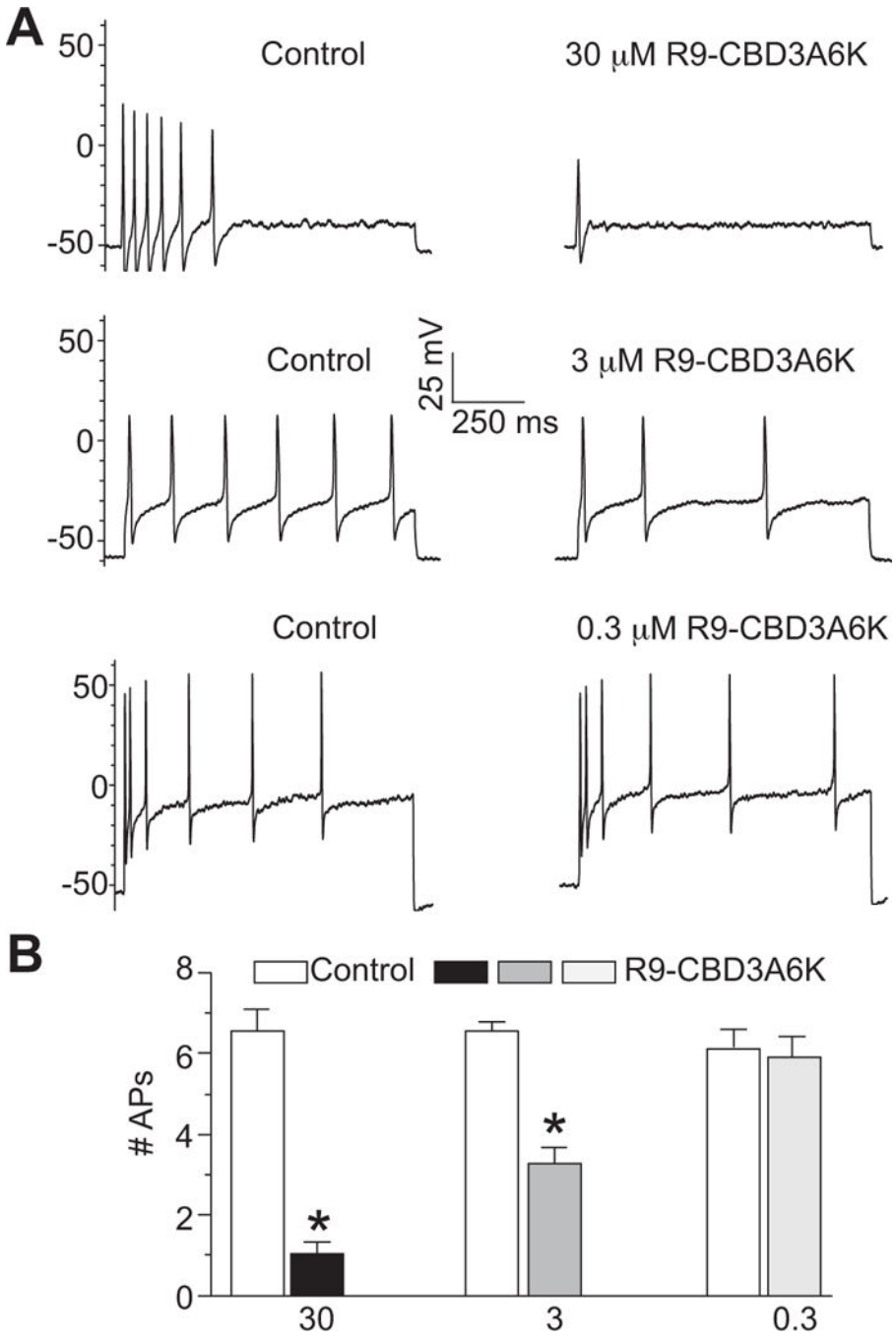

Figure 5. R9-CBD3-A6K peptides reduce the excitability of DRG neurons

Current clamp recordings were performed on small-to-medium (>30 μm – >40 μm, measured via a reticle) diameter lumbar 4–5 DRG neurons from naïve rats. Firing of 4–6 action potentials (APs) was elicited by a 1 second depolarizing current injection (ranging from 0.1 to 0.4 nA depending on the cell) every 30 seconds. (**A**) Representative recordings demonstrating that a concentration-dependent reduction in the number of elicited APs following application of 10 μM R9-CDB3-A6K. (**B**) Group data showing that R9-CBD3-

A6K caused a significant reduction in DRG action potential firing (*, $p<0.05$ versus control, Student's t-test; n=6–8 each).

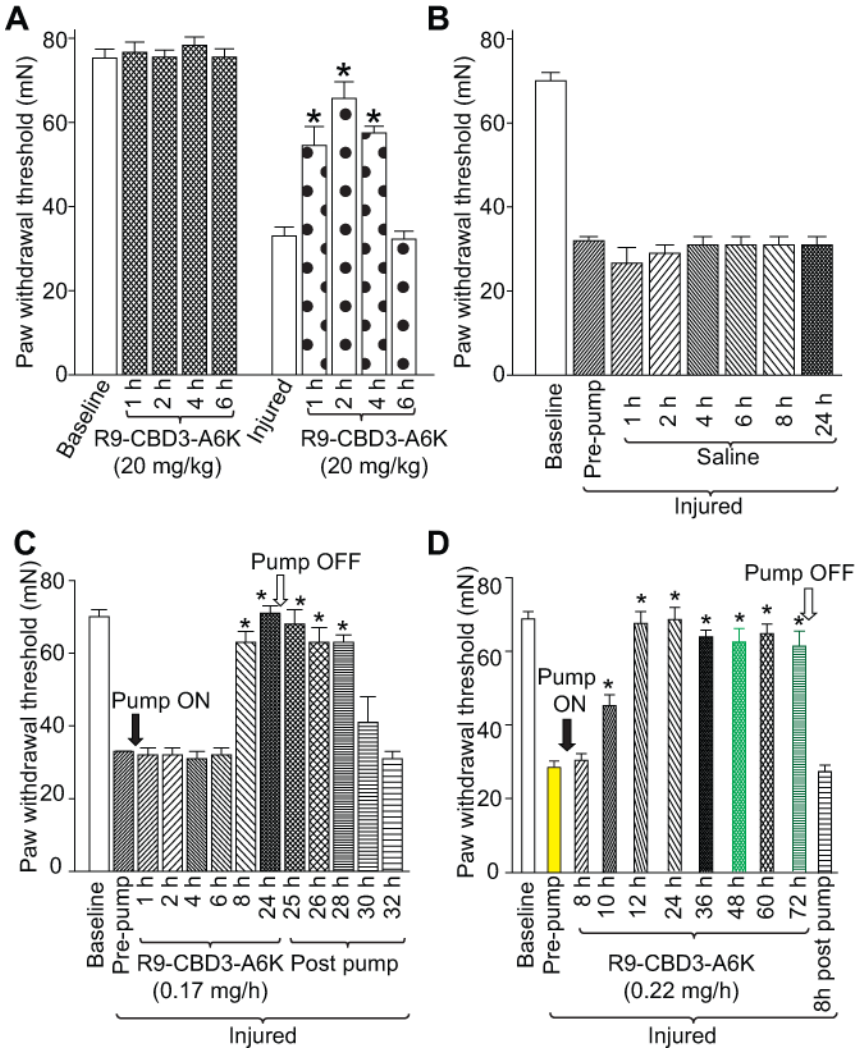

Figure 6. Acute and sustained administration of R9-CBD3-A6K reverses tibial nerve injury (TNI)-induced mechanical hypersensitivity

Paw-withdrawal thresholds (PWT in millinewtons, mN) were measured in nerve-injured rats before and after administration of R9-CBD3-A6K. PWT in rodents subjected to TNI was significantly reduced when compared to pre-surgery baseline at D14 post-TNI (n=6; white bar). (**A**) R9-CBD3-A6K, given as a bolus injection (20 mg/kg, i.p.), significantly reversed mechanical hypersensitivity at 1, 2 and 4 h post-dosing. (**B**) Tactile hypersensitivity of TNI rats was not lessened by chronic infusion of saline via an osmotic minipump. (**C**) Chronic administration of R9-CBD3-A6K (0.17 mg/h, s.c.) via an osmotic minipump, for 24 h, abolished the TNI-induced tactile hypersensitivity starting at 8 h post-dose and lasting for an additional 4 h after cessation of the pump. (**D**) Sustained administration of R9-CBD3-A6K (0.22 mg/h, s.c.) via osmotic minipump, for 72 h, provided continuous suppression of tactile hypersensitivity induced by TNI without any signs of development o tolerance. Mechanical hypersensitivity was assessed using the calibrated Von-Frey filaments. Behavior was tested at multiple time points indicated in the bar graphs. (*, $p<0.05$ compared to pre-dose (post-injury) baseline, One-way ANOVA with Dunnett's post hoc test). n=6 rats per condition.

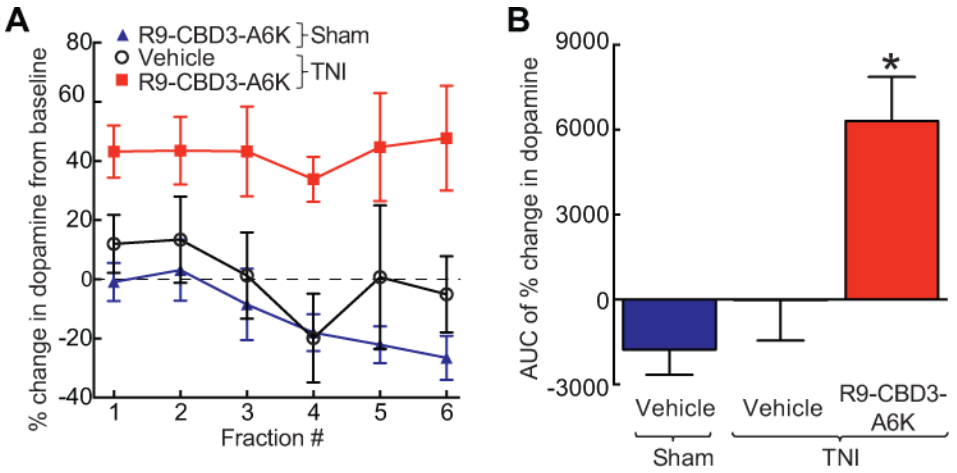

Figure 7. R9-CBD3-A6K induces dopamine (DA) release from nucleus accumbens (NAc) in TNI rats

(**A**) Extracellular DA levels in the NAc shell were measured via *in vivo* microdialysis in awake rats. Increase of DA release in all 6 fractions (total 3 h) after an acute administration of R9-CBD3-A6K (10 mg/kg, i.p.) was detected in rats with nerve injury (n=9). Vehicle administration did not produce any effect in rats with TNI (n=6). The same dose of R9-CBD3-A6K given to the sham-operated rats did not produce any effect (n=4). (**B**) The area under the time effect curve (AUC) also showed significantly higher levels of integrated DA release in TNI rats after R9-CBD3-A6K administration (*, $p<0.05$ comparing TNI/R9-CBD3-A6K vs. TNI/Vehicle or Sham/R9-CBD3-A6K, One-way ANOVA with Dunnett's post hoc test).

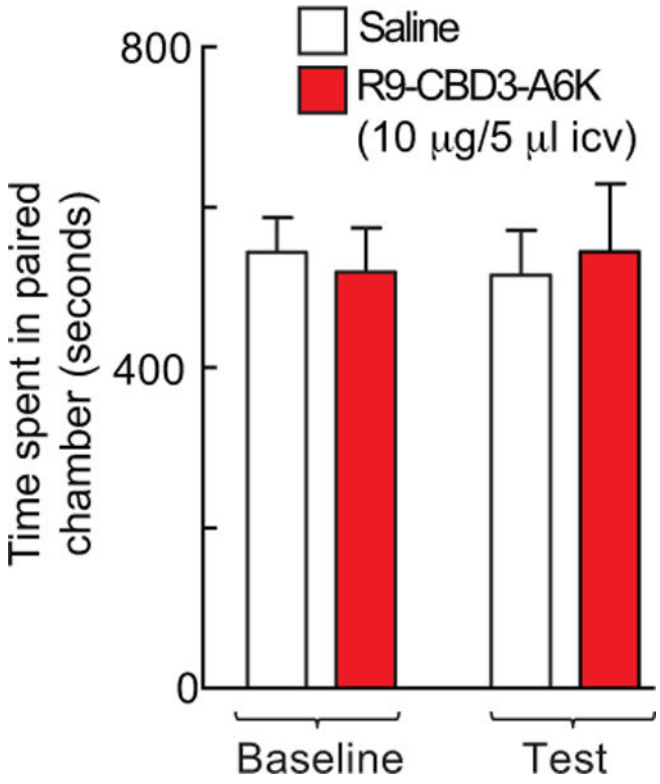

Figure 8. Absence of abuse liability by i.c.v. administration of R9-CBD3-A6K

Conditioned place preference (CPP) was used to determine the drug abuse liability of R9-CBD3-A6K. At baseline, all rats were allowed to explore all 3 chambers over a 20-minute period (total 1200 seconds). The animals were then confined to one side paired with drug administration and then the next day the opposite side paired with vehicle treatment for 30 min each. Total 5 exposures per treatment. 24 hours after the final exposure, all rats were allowed to explore all 3 chambers again and the total time spent in drug-paired chamber was measured in drug-free animals. R9-CBD3-A6K (10 μg in 5 μL, i.c.v.) did not produce any significant change in total time per chamber. ($p>0.05$ comparing baseline vs. test, Paired t-test). n=10 rats per condition.

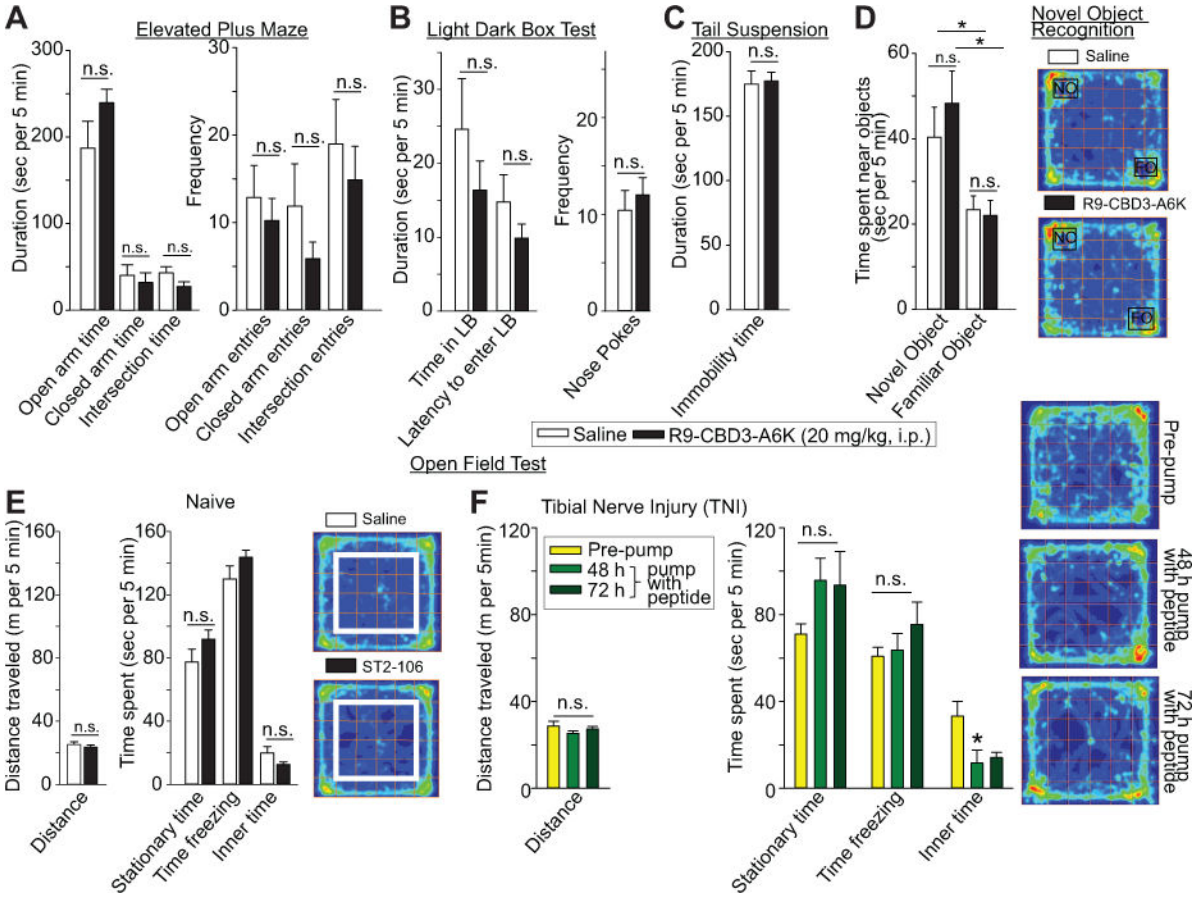

Figure 9. R9-CBD3-A6K treatment does not have CNS side effects

(**A**) Elevated plus maze to evaluate anxiety-associated behaviors revealed that R9-CBD3-A6K do not alter time spent or entries in the open, closed arms or intermediate zone. **(B)** Light dark box test to evaluate anxiety-associated behaviors revealed that R9-CBD3-A6K (20 mg/kg, i.p.) did not alter time spent in light box or latency to enter light box. (**C**) Tail suspension test of depression or despair-associated behaviors revealed that R9-CBD3-A6K (20 mg/kg, i.p.) did not alter the duration of immobility. (**D**) R9-CBD3-A6K (20 mg/kg, i.p.) and vehicle treated rodents both showed a similar preference for the novel object in a novel object recognition test. **(E)** R9-CBD3-A6K (20 mg/kg, i.p.) did not alter behaviors in an open field test (OFT) (n=8,8 for A-E). **(F)** R9-CBD3-A6K (~5.2 mg/day, s.c.) did not alter any behavior in a repeated daily (days 1, 3, 4) OFT in tibial nerve injury (TNI) rats with mechanical hypersensitivity, other than a decrease in time spent in the inner zone of OFT due to a reduction in novelty, n=4. Day 1 is the pre-pump day, when the rats exhibited mechanical hypersensitivity (see Fig. 6D, *yellow bar*)), day 3 is at 48 h after the start of the minipump, when the mechanical hypersensitivity was completely reversed (see Fig. 6D) and day 4 is at 72 h after the start of the minipump, when the mechanical hypersensitivity was completely reversed (see Fig. 6D).

Table 1

Percent of DRG neurons responding to constellation pharmacology triggers.

		0.002% DMSO		10 μM R9 CBD3 A6K	
Compound	**Final concentration**	**Number of cells**	**% of total**	**Number of cells**	**% of total**
Menthol	400 μM	64	5.4	48	3.7
Histamine	50 μM	36	3.0	35	2.7
ATP	10 μM	207	17.4	190	14.6
AITC	200 μM	21	1.8	16	1.2
Acetylcholine	1 mM	300	25.3	325	25.0
Capsaicin	100 nM	393	33.2	432	33.2
KCl	90 mM	1184	100.0	1301	100.0

The numbers are from two separate experiments for each treatment condition. Abbreviations: ATP, adenosine triphosphate; AITC, Allyl Isothiocyanate (mustard oil); KCl, potassium chloride.